Urban Heat Islands in Olomouc: A Geospatial Identification of Thermal Patterns, Urban Structure, and Human Perception

MASTER'S THESIS

submitted in partial fulfillment of the requirements for the degree
of

Master of Science (MSc)

PARIS-LODRON UNIVERSITY SALZBURG (PLUS)

Faculty of Digital and Analytical Sciences

Department of Geoinformatics

and

PALACKÝ UNIVERSITY OLOMOUC (UPOL)

Faculty of Science

Department of Geoinformatics

PLUS supervisor: Dr. Christoph Traun

UPOL supervisor: Dr. Jakub Koníček

submitted by

Annabelle Melanie Kiefer

Salzburg & Olomouc, July 2026

With the support of Erasmus+ programme of the European Union. This Master's Thesis has been developed in the framework of the Erasmus Mundus Joint Master Degree (EMJMD) "Copernicus Master in Digital Earth", jointly coordinated by Paris-Lodron University Salzburg, Department of Geoinformatics, Austria together with University of South Brittany, Computer Science Department, France and Palacký University Olomouc, Department of Geoinformatics, Czech Republic.

ANNOTATION

This diploma thesis aims to develop a transferable geospatial framework for urban heat island (UHI) risk assessment in the city of Olomouc, Czech Republic by integrating multi-source data on thermal conditions, socio-spatial characteristics and human perception. Conceptually, the approach is based on the climate risk framework proposed by the Intergovernmental Panel on Climate Change (IPCC), which defines risk as a function of hazard, exposure and vulnerability, with the latter further differentiated into sensitivity and adaptive capacity.

The proposed methodology combines satellite-based thermal data, in-situ air temperature measurements from an urban sensor network, participatory mapping results on thermal comfort and discomfort as well as socio-demographic and urban structure datasets. To ensure spatial comparability across heterogeneous data sources, all inputs are harmonized within a common spatial framework using a hexagonal grid, which enables consistent aggregation. The datasets are subsequently converted into indicators representing hazard, exposure, sensitivity and adaptive capacity, following widely used approaches in UHI vulnerability assessment.

To enable comparability between indicators with different value ranges, a normalization procedure is applied, and the indicators are then aggregated using a weighting scheme. Finally, UHI risk in Olomouc is visualized in static maps and interpreted with the definition of priority zones where UHI mitigation and adaptation strategies are most urgently needed. Furthermore, the most important insights of the analysis are highlighted in an interactive web mapping application, allowing decision-makers to gain additional insights into the distribution of UHI risk.

KEYWORDS

Urban Heat Island, Climate Risk Assessment, Land Surface Temperature, Thermal Comfort, Social Vulnerability, Geospatial Analysis

Number of pages: 54

Number of appendixes: 4

This thesis has been composed by Annabelle Melanie Kiefer for the Erasmus Mundus Joint Master's Degree Program in Copernicus Master in Digital Earth for the academic years 2024/2025 and 2025/2026 at the Department of Geoinformatics, Faculty of Natural Sciences, Paris Lodron University Salzburg, and Department of Geoinformatics, Faculty of Science, Palacký University Olomouc.

Hereby, I declare that this piece of work is entirely my own, the references cited have been acknowledged and the thesis has not been previously submitted to the fulfilment of the higher degree.

A. Kiefer

30.07.2026, Olomouc

Annabelle Melanie Kiefer

Acknowledgements

I would like to sincerely thank my supervisor Dr. Jakub Koníček for his guidance and support throughout the whole process of my thesis. His enthusiasm for my topic, the patience with which he answered all my questions, and his insightful feedback have been very helpful for the quality of my thesis.

I would also like to thank my co-supervisor Dr. Christoph Traun for his constructive feedback and insightful questions throughout the development of this thesis. His guidance encouraged me to reflect on my methodological choices and develop a critical mindset that significantly enhanced the quality of my work. Furthermore, I am grateful for the support provided by the Departments of Geoinformatics and Geography of Palacký University Olomouc, who provided me with valuable datasets and feedback. In this context, I would like to thank Veronika Květoňová, Michal Lehnert and Jaroslav Burian.

Palacký University Olomouc
Faculty of Science
Academic year: 2025/2026

ASSIGNMENT OF DIPLOMA THESIS

(project, art work, art performance)

Name and surname:	**Annabelle Melanie KIEFER**
Personal number:	**R241010**
Study programme:	**N0532A330010 Geoinformatics and Cartography**
Work topic:	**Urban Heat Islands in Olomouc: A Geospatial Identification of Thermal Patterns, Urban Structure, and Human Perception**
Assigning department:	**Department of Geoinformatics**

Theses guidelines

This diploma thesis examines the phenomenon of urban heat islands (UHIs) in Olomouc by integrating multi-source geospatial data. The core objective is to combine specialized temperature datasets—derived from thermal sensors, satellite imagery, and participatory mapping—with demographic information to identify, characterize, and interpret the most significant UHIs in the city. Particular attention is paid to examining correlations between spatial thermal patterns, the subjective perception of persons affected by heat and selected socio-spatial characteristics, including age distribution, population density, and land use typologies.

The analytical component encompasses the detection of thermal anomalies, their spatial delineation, and the exploration of their relationships with urban morphology and population structure. The results are visualised in the form of an interactive web mapping application, complemented, where appropriate, by dashboard elements.

Extent of work report:	**max. 50 pages**
Extent of graphics content:	**as needed**
Form processing of diploma thesis:	**electronic**
Language of elaboration:	**English**

Recommended resources:

PÁNEK, Jiří. 2016. 'From Mental Maps to GeoParticipation'. The Cartographic Journal 53(4):300–307. doi: 10.1080/00087041.2016.1243862.[3]
KRUM, Randy. Cool infographics: effective communication with data visualization and design. Indianapolis, IN: Wiley, 2014. ISBN: 9781118582305
DEBBAGE, Neil a J. MARSHALL SHEPHERD. The urban heat island effect and city contiguity. Online. Computers Environment and Urban Systems. 2015, vol. 54, s. 181-194. ISSN 0198-9715. Dostupné z: https://doi.org/10.1016/j.compenvurbsys.2015.08.002.
Květoňová, V., Pánek, J., Koníček, J., & Lehnert, M. (2025). Wintertime thermal perception in a central European city: the case of Olomouc, Czechia. Journal of Maps, 21(1). https://doi.org/10.1080/17445647.2025.2537687
Karam, R., Melchiori, M. "A Crowdsourcing-Based Framework for Improving Geo-spatial Open Data," 2013 IEEE International Conference on Systems, Man, and Cybernetics, Manchester, UK, 2013, pp. 468-473, doi: 10.1109/SMC.2013.85.
VOŽENÍLEK, V. (2002). Diplomové práce z geoinformatiky. Olomouc: Univerzita Palackého v Olomouci.

Supervisors of diploma thesis: Mgr. Jakub Koníček, Ph.D.
Department of Geoinformatics

Date of assignment of diploma thesis: October 1, 2025
Submission deadline of diploma thesis: July 30, 2026

L.S.

prof. RNDr. Martin Kubala, Ph.D.
Dean

prof. RNDr. Vilém Pechanec, Ph.D.
Head of Department

Olomouc November 3, 2025

CONTENT

LIST OF ABBREVIATIONS

Abbreviation	Meaning
AHP	Analytic Hierarchy Process
AR5	Fifth Assessment Report
ARD	Analysis Ready Data
AT	Air Temperature
CDSE	Copernicus Data Space Ecosystem
CHMI	Czech Hydrometeorological Institute
CLMS	Copernicus Land Monitoring Service
CZSO	Czech Statistical Office
EnCLOD	Enhancing governance Capacities of local authorities using Open Data
GIZ	Deutsche Gesellschaft für Internationale Zusammenarbeit GmbH
H3I	Human Heat Health Index
HEVA	Hazard-Exposure-Vulnerability-Adaptability
HI	Heat Index
HVI	Heat Vulnerability Index
IoT	Internet of Things
IPCC	Intergovernmental Panel on Climate Change
ISS	International Space Station
LCZ	Local Climate Zones
LST	Land Surface Temperature
MAUP	Modifiable Areal Unit Problem
NDVI	Normalized Difference Vegetation Index
NDBI	Normalized Difference Built-up Index
OSM	OpenStreetMap
PCA	Principal Component Analysis
PET	Physiologically Equivalent Temperature
PGIS	Participatory GIS
RTCS	Reported Thermal Comfort Score
RTDS	Reported Thermal Discomfort Score
S.L.	Soil Sealing *(Urban Atlas Classes)*
SUHI	Surface Urban Heat Island
SVF	Sky View Factor
TSV	Thermal Sensation Votes
UHI	Urban Heat Island
UHII	Urban Heat Island Intensity
UTCI	Universal Thermal Climate Index
WGBT	Wet Bulb Globe Temperature

INTRODUCTION

With progressing climate change, extreme heat is becoming one of the greatest global risks, exacerbated by increasing frequencies and intensities according to the IPCC. At the same time, ongoing urbanization processes are leading to increased temperatures and heat stress in urban areas. In this context, heat risk leads to serious health issues among residents, with approximately 489,000 global heat-related deaths annually between 2000 and 2019, which are often underreported (UNDRR, 2026). To make cities resilient and safe for their residents, the United Nations have therefore defined Target 11.b, emphasizing the importance of implementing policies focusing on climate mitigation and adaptation as well as holistic disaster risk management (United Nations, 2026).

In Europe, the latest heatwave period in June 2026, with record-breaking temperatures in central European countries such as Germany, Poland and the Czech Republic, has underlined the importance of tackling this issue (UNDRR, 2026). Europe is considered the world's most rapidly warming continent, with central European cities experiencing immense growth in heatwave temperatures (Guerreiro et al., 2018). Despite these rising temperatures, preparedness for extreme heat events remains low in many European countries, especially compared to the management of cold temperatures (Chen et al., 2025). This challenge is particularly pressing in the Czech Republic, where over 70% of the population already lives in cities, a share projected to rise to up to 94% by 2100. Heat risk in this context disproportionately affects elderly people, who currently make up one-fourth of the total population, with this share expected to grow further given the country's ageing population (Krkoška Lorencová et al., 2018).

Although UHIs are among the most intensively studied urban climate phenomena (T. R. Oke et al., 2017), existing research often examines the issue from a purely objective viewpoint, without taking into account the subjective perspectives of those affected. Since UHIs primarily impact the local population, it is crucial to also consider human perception of heat alongside the identification of population groups at particular risk, such as the elderly or children. This thesis therefore proposes a multi-source approach based on the climate risk framework of the IPCC, combining objective, subjective and socio-demographic data into indicators on hazard, exposure, sensitivity and adaptive capacity. Thereby, the approach helps to comprehensively understand the distribution of urban heat islands in the city of Olomouc and their effects on the population. The results in the form of static maps and an interactive web mapping application are aimed at supporting decision-makers in implementing sustainable urban planning solutions, both by counteracting the development of UHIs and by identifying areas where action is most urgently needed.

1 OBJECTIVES

This diploma thesis aims to examine the phenomenon of urban heat islands (UHIs) in Olomouc by integrating multi-source geospatial data. The core objective is to combine specialized temperature datasets, derived from thermal sensors, satellite imagery, and participatory mapping, with demographic information to identify, characterize, and interpret the most significant UHIs in the city. Particular attention is paid to examining correlations between spatial thermal patterns, the subjective perception of people affected by heat and selected socio-spatial characteristics, including age distribution, population density, and land use typologies.

Before conducting the actual analysis, thorough literature research was done to understand UHI concepts with a focus on social vulnerability and risk. In this context, this thesis implements a risk framework based on the definitions of the IPCC and guidelines from the *Deutsche Gesellschaft für Internationale Zusammenarbeit* (GIZ) *GmbH*. The practical part of this work is therefore guided by three main goals, each broken down into several sub-goals that build on one another.

The **first goal** concerns the preparation and harmonization of all indicators needed for the subsequent risk assessment. This requires establishing a common spatial framework using a hexagonal grid, processing each of the temperature, urban structure and socio-demographic datasets into this framework and harmonizing the resulting indicators through min-max normalization so that they become comparable despite their different original spatial resolutions and value ranges.

The **second goal** is the UHI risk assessment itself. Here, the first sub-goal is to conceptualize a transferable UHI risk model based on the components hazard, exposure, sensitivity and adaptive capacity, following the definitions of the IPCC and the guidelines of the GIZ. This model is then implemented for Olomouc by integrating the previously prepared indicators, after which UHI risk and its components are visualized and analyzed to determine areas with particularly high risk. As a final sub-goal, the resulting hazard component is validated against independent sensor network measurements to assess how well it reflects observed thermal conditions in the city.

The **third goal** is to compile the results of the risk assessment into an interactive web mapping application for decision-makers. This includes the creation of a dashboard that allows users to interactively explore UHI risk and a StoryMap that summarizes and communicates the most important results.

The results of this work will enhance UHI risk management in the city of Olomouc. The final web mapping application acts as both a reporting tool for the spatial distribution of UHI risk and as a planning tool for decision-makers to identify priority zones and implement suggested measures for UHI risk mitigation. These measures can have a long-term positive impact on society through improved well-being and health of residents, while also supporting more sustainable and resilient urban development, for example through reduced energy consumption.

2 STATE OF ART

This chapter introduces the concept of urban heat islands and how they can be measured using different temperature datasets derived from thermal sensors, satellite imagery and participatory mapping results as well as by integrating socioeconomic and demographic information. To efficiently combine the different objective and subjective data sources, UHI risk and vulnerability assessment are introduced, while the most relevant studies in this field are reviewed.

2.1 Urban Heat Island Concept

Urban Heat Islands (UHIs) can be defined as the temperature difference between urban areas and their surroundings (T. R. Oke, 1976). They are the most extensively studied urban climate phenomena, with their significance increasing over the past 25 years (Cheval et al., 2024), not least because their consequences lead to higher energy consumption in the form of increased cooling requirements and negative effects on residents in terms of heat stress. The formation of UHIs is closely linked to urban structure and human activity as well as weather conditions, with the ideal scenario being a cloudless sky and low winds. UHIs display enormous temporal variability and can occur in any season and time of day. They can be classified into different types based on the warming and cooling rates of the substrate, the surface and the air, namely subsurface urban heat islands, surface urban heat islands, canopy layer urban heat islands and boundary layer urban heat islands (T. R. Oke et al., 2017).

The canopy layer urban heat island, considering the near-surface layer, is the most frequently studied type in UHI research. Its formation depends mainly on street geometry, building fabric as well as anthropogenic heat from vehicle traffic and electricity use. The strongest urban heat islands in the canopy layer occur at night, making them a nocturnal phenomenon. Interestingly, at midday, the rural surroundings may have higher air temperatures than the urban area due to differences in the sky view factor (SVF), which indicates how much of the sky is visible from a given point (T. R. Oke et al., 2017). The low SVF in the street canyon leads to shading effects during the day, while at night, heat is trapped in the urban area (Tzavali et al., 2015).

Another frequently studied form of heat island is surface urban heat island (SUHI). Its formation heavily depends on geometric properties such as slope and angle of the surface as well as on exposure to the sun and sky. Similarly, the phenomenon is linked to radiative properties such as the ability to reflect shortwave radiation, known as albedo. Since many urban surfaces such as roofs have low albedo, SUHI is most pronounced during the day and in summer. In contrast to the nocturnal occurrence at the near-surface layer, SUHI is less prominent at night because the surfaces cool down immensely due to high SVF values (T. R. Oke et al., 2017).

To quantify UHI using a single metric, urban heat island intensity (UHII) or magnitude can be calculated, which corresponds to the difference between the highest urban temperature and the surrounding rural area (T. R. Oke, 1973; T. R. Oke et al., 2017). To consider the differences in geometric and radiative surface characteristics, it is recommended to use the Local Climate Zone (LCZ) scheme to quantify the intensity of heat islands. This scheme was introduced by Stewart and Oke (2012) and contains 17 zones that help classify the heterogeneity of urban areas. Each zone consists of similar surface structures, materials, land cover as well as human activity. In this context, the authors propose calculating UHI magnitude as the temperature difference between the categories LCZ 1 (Compact high-rise) and LCZ D (Low plants) (Stewart & Oke, 2012). Since LCZ 1 is often not a part of the urban structure of medium-sized Central European cities, LCZ 2 (Compact mid-rise) is considered instead (Lehnert et al., 2025).

2.2 Air Temperature and Land Surface Temperature

Air Temperature Measurements

There are different methods to identify UHI, which can mainly be divided into ground measurements, numerical simulations and remote sensing techniques. In this context, in situ measurements focusing on air temperature (AT) near the ground are most commonly used in literature (Cheval et al., 2024). To observe air temperature and understand UHI in the near-surface layer across the city, a network of thermometers with a respective sample size can be used, considering the complexity of urban and local climates (Lehnert et al., 2025; T. Oke, 1982; Stewart & Oke, 2012). In this context, it is important to ensure the availability of metadata of the sensors, especially with respect to the effects of weather (T. R. Oke et al., 2017).

Air temperature can be measured using a fixed approach with several weather stations representing the urban and rural LCZs (T. R. Oke et al., 2017). Savic et al. (2018) have used an urban network of 25 weather stations across nine LCZs to identify nocturnal UHII and heat wave risk in Novi Sad (Serbia) by comparing the results to mortality rates. While this can reveal temporal dynamics, a transverse approach by mounting a thermometer on a vehicle could also be considered when trying to understand local variations in urban form (T. R. Oke et al., 2017; Tzavali et al., 2015). Dobrovolný & Krahula (2015) have mounted a temperature sensor on the roof of a car with five-second measurements for nine sets between April 2011 and January 2012 to gain insights into nocturnal UHII in Brno. Lehnert et al. (2018) have carried out mobile measurements in the city center of Olomouc between July 2016 and February 2017 using a bicycle in order to identify hot and cool spots and to delineate spatial patterns according to LCZs.

To increase the sample size and better account for the heterogeneity of the urban structure, recent developments can also be found in the use of Internet of Things (IoT) architectures with low-cost, densely located participatory monitoring systems, measuring temperature data and accounting for the detection of UHIs (Fekih et al., 2020; Jang et al., 2024). Most often, studies focus on basic metrics such as daily mean, maximum and minimum temperature. In this context, Lehnert et al. (2025) have analyzed air temperature indices including summer days, tropical nights and UHII in Prague from two meteorological networks. They found that UHII is slightly higher in the summer during heat wave periods and that for summer nights, UHII is spatially less extensive compared to daytime distributions (Lehnert et al., 2025).

It is also possible to calculate additional thermal indices focusing on the effects on people to understand the thermal environment from a more holistic perspective. In fact, more than 160 thermal indices have been developed, where the Heat Index (HI) as well as the Universal Thermal Climate Index (UTCI) are some of the most commonly used ones (Středová et al., 2021). Kirschner et al. (2025) have calculated Wet Bulb Globe Temperature (WGBT), Physiologically Equivalent Temperature (PET), HI and UTCI to understand the relationship between these indices and thermal perception among park users in Prague on hot summer days. In this context, the results of the interviews with park visitors showed that thermal perception is strongly dependent on age and physical activity levels. While all thermal indices analyzed corresponded to the thermal perception of visitors, HI showed the most significant relationship (Kirschner et al., 2025).

Land Surface Temperature Measurements

Remote sensing techniques with the use of spatially continuous images of land surface temperature (LST) can give important insights into the formation of SUHI. These images can be acquired from drone data or satellites, with the most frequently used imagery sources being MODIS and Landsat (Cheval et al., 2024; Rodrigues de Almeida et al., 2021). In general, preprocessing regarding atmospheric and surface emissivity correction is required for these images (T. R. Oke et al., 2017). For Landsat specifically, several algorithms have been developed to retrieve LST from thermal infrared bands, such as the radiative transfer equation algorithm as well as the single and split window algorithm, which are generally based on the Planck blackbody radiation formula (Meng et al., 2021). Lehnert et al. (2021) have applied the split window and land-surface emissivity algorithm to process LST from Landsat 8 Surface Reflectance data. Alternatively, as has been done by Květoňová et al. (2024), the surface temperature of Landsat Collection 2 Level-2 can be used, which is analysis ready data (ARD) that has already been retrieved based on generalized emissivity from the Normalized Difference Vegetation Index (NDVI) (EROS Center, 2020).

Satellite data has a high spatial coverage and long-term temporal consistency, which helps to consider the heterogeneity of urban structure and to understand the changes in the development of SUHI over a long time period (Tzavali et al., 2015). On the other hand, the image acquisition is usually tied to a constant time of day with a low return rate of the satellite, meaning that the continuous development of heat islands cannot be analyzed in a way as it would be possible with the high temporal resolution of air temperature measurements (T. R. Oke et al., 2017). To reduce this issue and better understand the daily differences in SUHI formation, it is possible to use different imagery sources simultaneously. Květoňová et al. (2024) and Wei & Sobrino (2024) have combined Landsat 8 and 9 data with ECOSTRESS images, enabling analysis at different daytimes. Besides low return rates, LST cannot accurately represent the surface temperature at a street level in a street canyon, even when corrected towards thermal anisotropy, which needs to be considered when choosing a suitable study area and methodology (Květoňová et al., 2024; T. R. Oke et al., 2017).

Combining Air Temperature and Land Surface Temperature

Although air temperature and land surface temperature are both widely used to investigate urban heat islands, studies combining both datasets remain relatively limited. Due to their different strengths and limitations, a combination of both sources can provide a more comprehensive understanding of the urban thermal environment. However, these two sources cannot be directly compared due to the aforementioned differences in their daily behavior, SVF and surface properties (T. R. Oke et al., 2017; Voogt & Oke, 2003). In addition, the different spatial and temporal resolutions of both datasets need to be carefully considered when combining them.

Early attempts to integrate both approaches focused on combining ground-based and satellite observations. Fabrizi et al. (2010) used data from eight meteorological weather stations together with satellite-derived brightness temperatures to estimate near-surface air temperature and assess the spatial characteristics of UHI in Rome. Středová et al. (2021) investigated the interaction between AT and LST across LCZ and proposed a framework to derive the relationship between both variables. In this context, the authors also recommend synchronizing AT measurements with satellite overpasses to improve the comparability of both datasets. Žgela et al. (2025) combined authoritative and crowdsourced AT observations with earth observation-derived variables and urban morphology metrics to produce high-resolution air temperature maps, demonstrating the potential of remote sensing data to improve spatial modelling of urban air temperature.

Although UHI patterns derived from AT and LST are both based on temperature measurements, differences may occur because they represent different components of the urban thermal environment. In general, it is often assumed that locations with the highest air temperatures coincide with the highest surface temperatures. However, several studies have shown that this is not always the case and that the spatial distribution of maximum LST and AT may differ within heterogeneous urban landscapes (Geletič & Vysoudil, 2012; Středová et al., 2021).

2.3 Human Perception of Heat

Participatory Methods for Capturing Thermal Perception

Human perception is highly spatial, which is why GIS is becoming increasingly important in citizen participation, especially in areas such as mobility, walkability, public safety and thermal comfort. Engaging the community not only helps to gain valuable insights into their lived experience, but also to raise awareness about a specific phenomenon and to ensure a democratization of science (Alonso & Renard, 2019). In the context of UHIs, human perception is a crucial component to understanding how individuals perceive their thermal environments. While commonly used objective measures such as AT or LST measurements provide insights into physical heat patterns, they do not consider personal factors at a human scale, which highlights the importance of integrating human experience into the spatial analysis of urban heat.

To capture thermal perception, several techniques have been developed, including qualitative and quantitative participatory methods, which each offer specific advantages and limitations depending on the study aims and target group. For instance, stakeholder workshops and focus group discussions can be used to map vulnerable areas in a city (Krkoška Lorencová et al., 2018). These particular methods are also often used to engage professionals in the context of risk and vulnerability assessment, where subjective weightings for different indicators can be defined by independent experts and affected population groups (Sidiqui et al., 2022). Furthermore, it is also possible to focus on particular target groups, as has been done by Lim et al. (2022) by integrating youth as the new generation whose lives will be largely affected by the negative effects of UHIs and heatwaves.

Another commonly used method is participatory mapping campaigns capturing long-term experiences of the population. They offer qualitative insights into individual thermal perception with thermal comfort and discomfort. In general, they can be conducted on various scales, although these campaigns often do not contain a very high spatial and temporal precision that would be necessary for a street-level analysis (Květoňová et al., 2024). Usually, respondents are asked to mark points or polygons on a map, either paper-based or online. In many studies, especially in the Czech Republic, the web application *EmotionalMaps* by Pánek (2019) has been used. At the same time, paper-based questionnaires requiring manual digitization a priori are still commonly used, as they ensure to include citizens such as the elderly, who are unfamiliar with web applications. To increase the qualitative insights, an accompanying questionnaire is often part of the campaign. While the survey can include general demographic questions regarding gender, age, education and economic status, it can also deliver crucial additional insights beyond the actual location into why people feel thermally comfortable or uncomfortable (Pánek, 2019).

In contrast, thermal walks can be used to provide real-time evaluation of thermal conditions under controlled circumstances. Participants evaluate their thermal environment while walking at a predefined time that is tailored to extreme thermal conditions. External factors such as the pace while walking or the clothing of participants are equalized to ensure comparability between participants. To capture the real-time, subjective perceptions of the respondents, tools such as Esri ArcGIS Survey123 can be used. Compared to participatory mapping campaigns, this method is based on a small number of respondents, which is why a wide range of ages or health conditions can often not be considered (Květoňová et al., 2024).

Similarly, this method is often conducted on a neighborhood scale that is walkable for the participants, which is why this technique can often not provide the necessary insights for a city-scale analysis. While participatory mapping campaigns mostly offer insights into thermal perception, thermal walks rather analyze thermal sensation that can be described as a conscious feeling of the respondents. In this context, a commonly used metric is thermal sensation votes (TSV). Due to the aforementioned strengths and limitations of participatory mapping campaigns and thermal walks, both methods can be combined to gain insights into real-time and long-term thermal experiences as has been done by Květoňová et al. (2024).

Applied Studies in Participatory Mapping

Regarding the integration of multi-source data to gain a more holistic understanding of the spatial distribution of thermal comfort and UHIs, several studies have combined participatory mapping results with objective measures. Lehnert et al. (2021) conducted a participatory mapping campaign in Plzeň and Olomouc between May and October 2020 and compared the results with LST measurements, finding that LST hotspots mostly differed from mental thermal hotspots and coolspots. Building on this campaign, Lehnert et al. (2023) identified citizens' preferred heat-mitigation measures, finding that trees, parks and combinations of greenery with blue elements were most favored.

Most recently, Květoňová et al. (2025) investigated wintertime thermal perception in Olomouc, finding that residents perceive cold near rivers and in open windy areas. Interestingly, thermally uncomfortable areas often remain across seasons, which is why measures such as green infrastructure can improve thermal comfort for both summer and winter. In Prague, Květoňová et al. (2024) analyzed heat threat using a thermal walk and participatory-based cognitive mapping alongside satellite imagery from Landsat and ECOSTRESS, finding an overall low agreement between the three methods with only a few major hotspots and coolspots identified consistently across all of them. Together, these studies show a clear demand for further investigation into understanding the mismatches between perceived and meteorologically obtained conditions.

Participatory mapping is especially important in vulnerability assessment, where local knowledge can give crucial insights beyond commonly used datasets. In this context, community engagement can help to raise awareness of risk and fuel solution-based thinking. Sullivan-Wiley et al. (2019) used focus group discussions to gain insights into concerns about environmental, social and hybrid risks in villages in Uganda as well as participatory mapping exercises to map these risks. With this combination of spatial and non-spatial methods, the authors try to account for risk and vulnerability components that cannot be mapped, especially regarding social norms (Sullivan-Wiley et al., 2019). Similarly, Canevari-Luzardo et al. (2017) applied a partial participatory GIS (PGIS) approach in small Caribbean communities in Grenada, combining community vulnerability mapping with geo-referenced household data through an external facilitator who handled the technical GIS aspects of the process. Their results demonstrate that participatory mapping methods can support knowledge co-production and stakeholder engagement, helping communities record local spatial knowledge on vulnerability and hazards while supporting the development of disaster risk management strategies.

2.4 UHI Risk Assessment and Social Vulnerability

To gain a holistic understanding of the UHI phenomenon and its impacts on the population, social vulnerability can be assessed within a climate risk framework. In general, social vulnerability increases in densely populated areas, where there is a high proportion of socioeconomically or age-related vulnerable populations (Ming et al., 2024; Vaňo et al., 2025). Especially the elderly have a reduced ability to thermally regulate, which is why heat-related diseases and mortality during heat waves are very common for this population group (Cheng et al., 2021).On the other hand, young people can be vulnerable to heatwaves due to lower sweating rates and women due to biological differences and a higher proportion of non-workers, largely contributing to unpaid care work (Abrar et al., 2022; Alonso & Renard, 2020). These findings highlight that urban heat impacts result from the interaction of thermal conditions, population distribution, and socio-demographic characteristics, which is why the integration of these diverse factors into a coherent analytical framework is crucial.

Vulnerability Frameworks

Vulnerability assessment is becoming increasingly important for different climate hazards, not least due to the recommendations of the IPCC. Particularly concerning the risk assessment of heatwaves, the number of published papers has increased drastically since 2019, with China leading the way with most research in this field (Xu et al., 2025). A widely conceptualized framework for heat wave risk assessment is Crichton's risk triangle, which distinguishes between hazard, exposure and vulnerability (Crichton, 1999). In addition, the heat vulnerability index (HVI) has been used in many studies. This index builds on Crichton's risk triangle, but includes a fourth component, referred to as adaptive capacity (Szagri et al., 2023).

Since the HVI is purely static in nature, the hazard-exposure-vulnerability-adaptability (HEVA) framework was introduced by Xu et al. (2025) as an alternative to assess heat risk holistically and enable proactive urban planning. This framework is especially suited for high-resolution spatial analysis and considers hazard based on real-time thermal metrics, exposure as population density, vulnerability as socio-demographic sensitivity and adaptability as cooling infrastructure and healthcare access. Its strength lies in the integration of dynamic adaptability metrics and socio-spatial inequalities, which ultimately help to precisely define high-risk areas as important measures in urban planning for UHI mitigation (Xu et al., 2025). Similarly, Kamath et al. (2023) have argued that the use of LST can overestimate HVI during the day, which is why they propose the human heat health index (H3I). This index incorporates remote sensing data, mobile traverse measurements, climate models and a census-tract-based social vulnerability index to accurately assess urban heat vulnerability during the day. Moreover, they emphasize the importance of engaging the community and gathering their feedback on heat hotspots in the city to develop heat mitigation strategies that address the specific needs of residents in different neighborhoods (Kamath et al., 2023).

Another widely used methodology is the natural risk framework introduced by the IPCC, where there is no single, uniform definition of vulnerability due to the availability and use of several versions. In this context, the Fourth Assessment Report (AR4) defines vulnerability as exposure, sensitivity and adaptive or coping capacity (IPCC, 2007). While this approach continues to be used in most studies analyzing UHI risk and vulnerability (Abrar et al., 2022; Bhattacharjee et al., 2019; Vaňo et al., 2025), the Fifth Assessment Report (AR5) introduces a new definition excluding exposure from vulnerability. Instead, this methodology defines climate risk based on hazard, exposure and social vulnerability, with the latter further subdivided into sensitivity and capacity to cope or adapt (IPCC, 2014). To enhance standardization in vulnerability and risk assessment based on these frameworks, the GIZ has published guidelines as the *Vulnerability Sourcebook* (GIZ, 2014) and as a *Risk Supplement to the Vulnerability Sourcebook* for the AR5 (GIZ and EURAC, 2017), which will be followed in the scope of this thesis.

Hazard can be defined as the climatic phenomenon of UHI, exposure as the population and elements at risk and vulnerability as characteristics of exposed elements (Räsänen et al., 2019). In this context, sensitivity focuses on the extent to which a population is affected by heat, which depends primarily on age, gender, ethnicity and socioeconomic characteristics (Buzási, 2022; IPCC, 2014). Regarding the capacity to cope or adapt, most studies focus exclusively on adaptive capacity, as the long-term ability to adjust to future conditions can be reliably measured using spatial data. However, other studies suggest considering coping capacity instead, thereby analyzing the ability to deal with the immediate impacts of heat-related climate risks (Quesada-Ganuza et al., 2023). Using the AR5 framework, a distinction can be made between vulnerability maps, which focus primarily on demographic and socioeconomic data as well as risk maps, which consider all of the aforementioned components (Räsänen et al., 2019).

Indicator Selection

When analyzing risk and social vulnerability, the first step is always to select suitable indicators for each component. A wide range of indicators has already been used in this context, with discrepancies arising from the various risk and vulnerability frameworks, especially due to the differences between the IPCC's AR4 and AR5. According to AR5, hazard is mainly described using a temperature dimension, which can be determined using LST or AT measurements, while a duration dimension with a longer temporal extent is also possible, thereby enabling the creation of indices such as the number of summer days or tropical nights (Thanvisitthpon, 2023). Wu et al. (2024) have defined hazard as maximum daytime and nighttime surface temperature, the number of extremely hot days and the frequency of heatwaves, whereas Ellena et al. (2023) relied solely on the distribution of UHIs.

In both the AR4 and AR5 frameworks, exposure is mainly described based on general population density (Abrar et al., 2022; Thanvisitthpon, 2023; Vaňo et al., 2025; Wu et al., 2024), but it is also possible to focus exposure exclusively on the vulnerable population, as was done by Ellena et al. (2023) including the over 65 years population. Given the nocturnal nature of UHIs, population distribution during the night can also be a key indicator of exposure (Reinwald et al., 2024). In addition, Sidiqui et al. (2022) included impervious surfaces and Thanvisitthpon (2023) incorporated land use types in the exposure component, with urban areas and ongoing urbanization exacerbating the UHI phenomenon. In this context, it should be noted that the assignment of indicators to specific components can be ambiguous. Comparing the two cited studies above, Sidiqui et al. (2022) assign building density to the exposure component, while Thanvisitthpon (2023) defines it as sensitivity.

Most indicators can be found for vulnerability in the context of sensitivity and adaptive capacity, not least since several studies focus exclusively on these components. In terms of sensitivity, vulnerable age groups are the most common indicators, with the threshold for the elderly negatively affected by UHI effects set at 65 years old (Abrar et al., 2022; Bhattacharjee et al., 2019; Buzási, 2022; Räsänen et al., 2019; Vaňo et al., 2025b; Wu et al., 2024). On the other hand, there is no clearly defined threshold for the very young population, which is vulnerable to UHIs. Here, young people can be defined as those aged below two to nine years (Abrar et al., 2022; Buzási, 2022; Sidiqui et al., 2022), fourteen (Bhattacharjee et al., 2019; Vaňo et al., 2025) or even eighteen (Räsänen et al., 2019). Besides age, gender can also be an important factor, with the female population in general, or more precisely women over the age of 65, considered to be at risk (Abrar et al., 2022; Ellena et al., 2023; Räsänen et al., 2019). Additional indicators in this component focus on socioeconomic indicators such as low-income households (Räsänen et al., 2019; Thanvisitthpon, 2023) or low level of education (Abrar et al., 2022; Ellena et al., 2023; Räsänen et al., 2019). Another important category in this context is preexisting medical conditions such as the distribution of people with heart diseases (Ellena et al., 2023) or people taking medication (Sidiqui et al., 2022), although there is often a lack of data for these indicators.

Lastly, adaptive capacity often focuses on medical facilities and the availability of relevant practitioners, since these facilities are crucial for treating people affected by heatwaves (Abrar et al., 2022; Sidiqui et al., 2022; Varquez et al., 2025). This specific example once again highlights the ambiguity and complexity of assigning an indicator to a particular component. While some studies argue that medical facilities are necessary for adapting to the negative effects of UHIs and therefore have a positive impact on the final risk map, these locations can also be viewed as vulnerable infrastructure where vulnerable groups, especially the elderly and people with ill health, are concentrated (Reinwald et al., 2024). Another important aspect of adaptive capacity are green spaces, specifically their proportion relative to impervious surfaces and their accessibility (Sidiqui et al., 2022; Thanvisitthpon, 2023). For this purpose, biophysical indices such as the NDVI or Normalized Difference Built-up Index (NDBI) can be used (Abrar et al., 2022; Bhattacharjee et al., 2019; Buzási, 2022). Especially in hot climates, the availability of air conditioning and proximity to public places such as shopping centers and libraries with air conditioning are also of crucial importance (Ellena et al., 2023; Wu et al., 2024).

Methodological Considerations

Regarding data acquisition and data preparation, it is important to consider zoning, meaning the differences in spatial units that can lead to different spatial patterns of vulnerability. In general, the aggregation of spatial data leads to the modifiable areal unit problem (MAUP), where the same underlying data produce varying results when averaged over different boundaries (Räsänen et al., 2019). Usually, socio-economic data is aggregated to common administrative boundaries or census tracts, which is why risk assessment is often conducted on the corresponding levels. Ellena et al. (2023) and Voelkel et al. (2018) have conducted UHI risk and vulnerability assessment on the census tract level, while Savic et al. (2018) and Buzási (2022) have used city districts as the spatial unit. As an alternative to administrative boundaries, geons introduced by Lang et al. (2014) can be used, which try to build optimal areal units.

In this context, Räsänen et al. (2019) compared different zoning options of socioeconomic data at common statistical units in Finland such as municipalities, administrative areas and postal code areas. After resampling vulnerability and hazard to 250 m grid cells to ensure the comparability of the different components, they found that zoning has a large effect on vulnerability maps, thereby recommending the use of finer spatial units when integrating socioeconomic data. After preparing the different indicator datasets, it is important to find a suitable normalization technique since the indicators have different value ranges. Min-max normalization is one commonly used technique, where the values of either hazard, exposure or vulnerability indicators are divided by the maximum value of each corresponding indicator (GIZ, 2014; Räsänen et al., 2019).

Since the synthesis for risk assessment is based on many different indicators, it is important to consider different weighting options. These can mainly be divided into the overlay method, subjective weighting, objective weighting and combined weighting (Xu et al., 2025). The overlay method assuming equal weights has been widely applied, but the method does not consider varying impacts of different indicators and can therefore limit the accuracy of the results. Subjective weighting considers expert-based knowledge assigning weights to different indicators and includes methods such as Analytic Hierarchy Process (AHP) or the Delphi method (Xu et al., 2025).

Alonso & Renard (2020) conducted AHP around a four-step hierarchical procedure, describing the vulnerability factors, gathering pairwise comparisons from an expert panel, checking the consistency of their responses and aggregating the results into vulnerability weights. On the other hand, Räsänen et al. (2019) have used the Delphi method for assigning subjective weights on vulnerability determinants using a panel with experts dealing with climate change impacts in Helsinki. Nonetheless, these weighting options are inherently subjective, which is why an alternative can be objective weighting or combined weighting integrating the strengths of both subjectivity and objectivity. Objective weighting methods determine the weights of indicators based on actual data, including methods such as principal component analysis (PCA), which has been used by Abrar et al. (2022).

Similarly, to establish comprehensive evaluation models, different methods have been implemented on how to aggregate hazard, exposure, sensitivity and adaptability. In general, it is possible to either multiply and divide the different components or add and subtract them (Xu et al., 2025). Ellena et al. (2023) have multiplied hazard, exposure and vulnerability to obtain a single risk value per census tract, which was then normalized and categorized. Contrary, the *Vulnerability Sourcebook* suggests using weighted arithmetic aggregation, where the indicators are weighted, summed and then divided by the sum of their individual weights (GIZ, 2014).

In this context, maps are commonly used to visualize risk and vulnerability, where specific design choices influence how well they are understood by decision-makers. De Groot-Reichwein et al. (2018) evaluated different mapping techniques and found that choropleth maps were preferred over isopleth maps by policymakers. Color hue was also favored as the graphic variable, particularly for sequential schemes and comparing multiple scenarios, in which context the authors also created an interactive atlas. For the classification of values within these maps, different methods can be applied, such as quintiles (Räsänen et al., 2019) or the Jenks natural breaks algorithm, which Ellena et al. (2023) used to group hazard and exposure values into distinct classes. Besides maps, additional visualization techniques such as graphs, charts or an evaluation matrix combining risk factors can be considered (GIZ, 2014; GIZ & EURAC, 2017). Since vulnerability and risk are inherently dynamic, it is further recommended to integrate projections of future changes into these assessments, rather than relying solely on static representations of present conditions (Räsänen et al., 2019).

2.5 Research Gaps

Many studies analyzing UHI risk operate on the city scale, but typically rely on administrative boundaries such as city districts (Buzási, 2022; Savic et al., 2018) and census tracts (Ellena et al., 2023; Voelkel et al., 2018) or compare different administrative levels against each other. However, these units do not necessarily reflect actual urban structure and are prone to the MAUP, as the choice of zoning can considerably alter the resulting spatial patterns (Räsänen et al., 2019). To address this, a hexagonal grid is here established as the spatial framework, independent of existing administrative boundaries.

This study is further complemented by the ongoing EnCLOD (Enhancing governance Capacities of Local authorities using Open Data) project, co-funded by the European Union through the Interreg Central Europe programme, with the city of Olomouc being one pilot area implementing a network of sensors to monitor UHIs and traffic, thereby aiming to support enhanced public administration through open data. As part of the project, microzones have been introduced as an alternative to administrative units, being delineated according to real urban conditions such as traffic flow and land use. They are here used as a second spatial framework for the visualization and analysis of UHI risk. While most risk assessments validate their models only by comparing different methodological choices against each other (Räsänen et al., 2019), this thesis makes use of the EnCLOD IoT sensor network to validate the hazard component against sensor measurements from ten weather stations.

Existing studies tend to focus either on physical measurements of UHIs or on isolated aspects of human perception and the integration of human perception into climate risk and vulnerability mapping remains only slightly observed (Canevari-Luzardo et al., 2017; Sullivan-Wiley et al., 2019). Lehnert et al. (2021) found that LST hotspots mostly differed from mental thermal hotspots and coolspots, and Květoňová et al. (2024) similarly found only a low agreement between thermal walks, cognitive mapping and satellite-derived measures, together showing that physical heat patterns alone cannot capture how heat is experienced. Participatory mapping results can therefore add substantial value beyond objective datasets, helping identify vulnerable areas and raise awareness (Alonso & Renard, 2019). Therefore, this study combines participatory mapping results from an existing campaign in Olomouc with satellite and demographic data to gain a more holistic understanding of UHI risk.

Since there are discrepancies between UHI risk frameworks regarding indicator selection and aggregation methods that make comparisons between study areas difficult (Ellena et al., 2023; Sidiqui et al., 2022; Thanvisitthpon, 2023), this study aims to develop a standardized and transferable UHI risk model, based largely on the recommendations of the GIZ Vulnerability Sourcebook and its Risk Supplement (GIZ, 2014; GIZ & EURAC, 2017). Finally, while some studies have moved away from purely static visualizations, such as the interactive atlas developed by de Groot-Reichwein et al. (2018) to communicate UHI impacts to policy-makers, tools that combine risk visualization with actionable insights for local decision-makers remain rare. This study therefore compiles its results in an interactive web mapping application, including a dashboard to support UHI risk communication and adaptation planning in Olomouc.

3 METHODOLOGY

This chapter introduces the study area and its relevance in the context of UHI analysis. Furthermore, the different data sources used in this study are introduced. Lastly, the software used as well as the processing procedure are explained.

3.1 Study Area

Olomouc is located in central Moravia in the eastern part of the Czech Republic and is the sixth largest city in the country with a population of 103,000 inhabitants (CZSO, 2025). Of its total population, over one third can be considered vulnerable groups, with 16% of the population being under the age of 14 and 20% over the age of 65 (CZSO, 2021). The urban structure of the city is complex and can be traced back to the 10th century, with a densely populated historical city center surrounded by a belt of parks that offer relevant green spaces (Lehnert et al., 2021; Wagner et al., 2025).

In total, Olomouc covers an area of 103 km², where 55% is agriculturally used and 11% is considered forested land (CZSO, 2024). Built-up areas in Olomouc can be mainly found as apartment blocks in older residential areas or recently developed residential areas in the suburbs (Lehnert et al., 2021). According to the Urban Atlas Land Cover/Land Use classification, 9% of the city can be considered as continuous urban fabric with soil sealing (S.L.) over 80%, 4% are discontinuous dense urban fabric (S.L. 50%-80%) and 12% consist of industrial or commercial units (CLMS, 2021a).

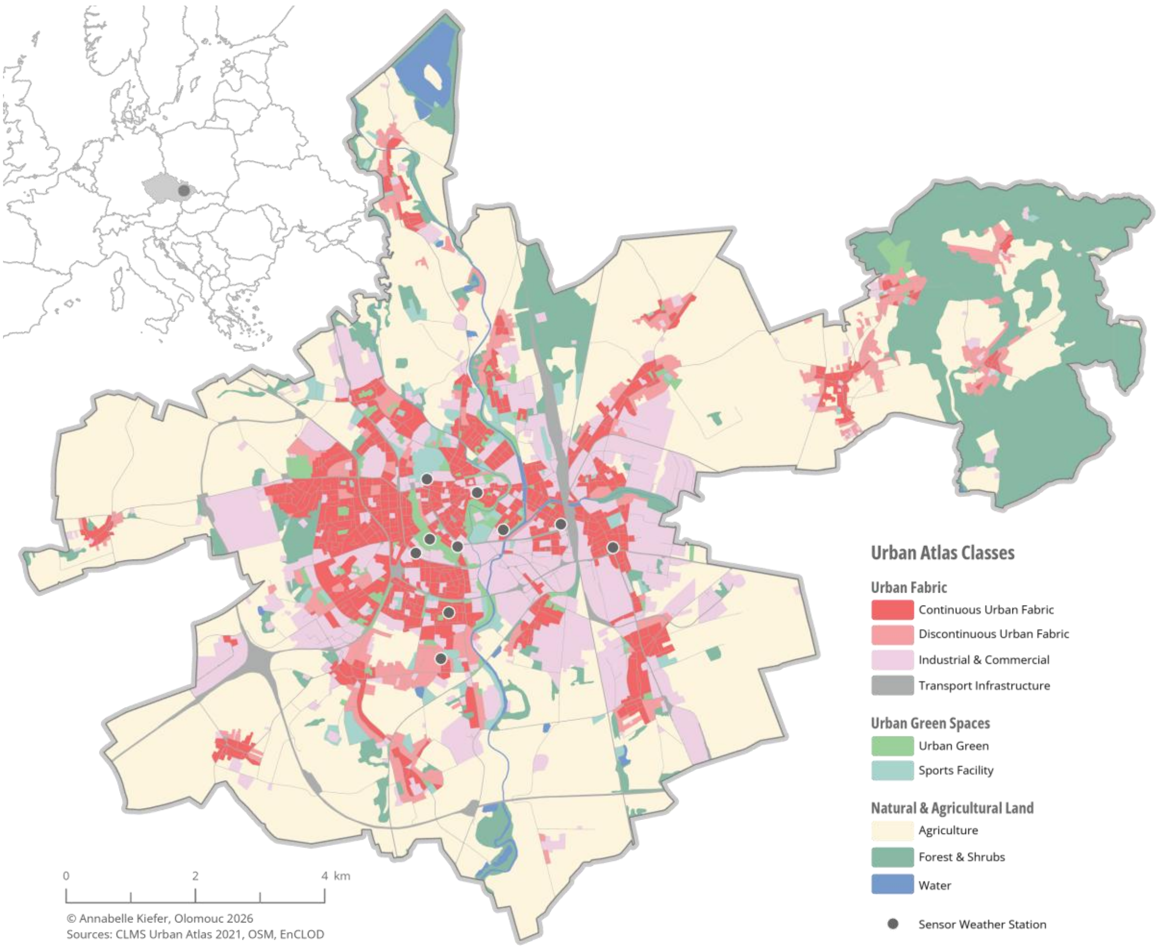

Figure 1 Study area of Olomouc classified according to CLMS Urban Atlas 2021.

Olomouc has a Cfb climate according to Köppen-Geiger climate classification, indicating warm summers with an average temperature below 22°C and relatively constant precipitation throughout the whole year (Geiger 1961). The mean monthly air temperature ranges from -0.1°C in December to 19.7°C in July, with a mean annual precipitation of 715mm (Climate Data, 2026). For the summer period of 2025 (late June to end of September), 44 summer days with a maximum air temperature over 25°C as well as 16 warm nights with a minimum temperature over 17°C were measured in Olomouc using the sensor network (Table 1). Correspondingly, there were three heatwaves with maximum temperatures over 30°C, with the longest one lasting between August 13 and August 16. In this context, the highest temperature was measured on August 15 with 34.54°C at Fischerova weather station in the early afternoon.

Table 1 Temperature statistics for ten weather stations of the sensor network. The location of the sensors can be found in Figure 1.

Weather Station	Mean Temperature	Maximum Temperature	Maximum Apparent Temperature	Summer Days	Warm Nights
Fischerova	19.39	34.54	35.06	47	18
Flora	19.35	34.36	34.94	45	18
Fugnerova	19.18	34.51	35.01	47	14
Nádraží	19.16	33.19	34.25	41	19
Nám. Republiky	19.03	34.11	34.39	36	14
Smetanovy sady	18.92	34.03	34.96	44	12
Trnkova	19.24	34.40	35.07	46	19
Tržnice	19.64	34.14	34.57	48	20
U Letadla	19.39	34.47	34.90	47	16
UPOL	19.11	34.12	34.78	45	15
Mean	19.24	34.19	34.79	44.6	16.5

3.2 Data

To create the indicators necessary to conduct the UHI risk assessment, several data sources had to be utilized, which can mainly be divided into temperature datasets, data on urban structure and socio-demographic data.

Temperature Datasets

For the thermal component of this study, LST data from the ECOSTRESS module located on the International Space Station (ISS) at a spatial resolution of 70m was acquired using the AppEEARS platform from NASA, where a total of 15 representative scenes were selected. Additionally, sensor network data on temperature, relative humidity, air pressure as well as wind direction and speed from 10 weather stations in Olomouc were acquired for the summer period 2025. The data were queried from the IoT register Data portal using 15 min intervals, resulting in over 90,000 measurements that were further processed in RStudio. To calculate UHII with the sensor network measurements, temperature data from Olomouc Holice as a rural reference station were downloaded at a daily interval for the same time period from CHMI.

To also consider subjective perception of thermal patterns, participatory mapping results on thermal comfort and discomfort were provided by the Geography Department of Palacký University Olomouc. The dataset is based on a participatory mapping campaign carried out between May and October 2020 and consists of 1,423 polygons and 668 point features, giving thorough insights into how temperature is perceived by residents of Olomouc during summer.

Table 2 Overview of temperature datasets used in this study.

Dataset	Source	Temporal Resolution	Spatial Resolution
ECOSTRESS Gridded Land Surface Temperature and Emissivity Instantaneous L2 Global 70 m V002	Hook, S., & Hulley, G. (2023)	June – September 2025	70m
Meteorological data from 10 weather stations in Olomouc	CiTiQ & EnCLOD (2026)	June – September 2025 (15 min)	Point
Meteorological data from Olomouc, Holice	Czech Hydrometeorological Institute (CHMI) (2026)	June – September 2025 (daily)	Point
Participatory Mapping results	Lehnert et al. (2021)	May – October 2020	Point, Polygon

Urban Structure

To identify urban structure in the study area, Urban Atlas Land Cover/Land Use 2021 as well as Urban Atlas Street Tree Layer 2021 from the Copernicus Land Monitoring Service (CLMS) have been downloaded as shapefiles via the Copernicus Data Space Ecosystem (CDSE). In addition, data on LCZ at a spatial resolution of 100m was provided by the Geography Department of Palacký University Olomouc under the supervision of Michal Lehnert. This dataset was later used to calculate UHII from LST data by distinguishing reference pixels of LCZ D (Low plants).

To better understand the distribution of vulnerable infrastructure such as schools, kindergartens and hospitals, OSM point data on these attributes was acquired using QGIS. For the adaptive capacity component, data on health service providers was downloaded from the National Register of Health Service Providers as a CSV table, which was later processed in Google Colab for efficient integration of the dataset as a point layer in ArcGIS Pro.

Furthermore, microzones, which were developed as part of the EnCLOD project for several central European cities, were integrated into the analysis. They are based on basic settlement units and combine areas with similar characteristics in urban structure, traffic and socioeconomic characteristics, thereby offering a finer delineation of urban space than conventional administrative boundaries. Within this study, microzones were primarily used for visualization purposes and to aggregate hexagon-based risk results to gain insights into the areas in the city most affected by heat events.

Table 3 Overview of datasets on urban structure used in this study.

Dataset	Source	Temporal Resolution	Spatial Resolution
Healthcare services provided in Olomouc	Czech Data Portal (2026a)	March 2026	Point
Local Climate Zones (LCZ) of Olomouc	Department of Geography, Palacký University Olomouc	2026	100m
Microzones	EnCLOD	2025	Polygon
Urban Atlas Street Land Cover/Land Use 2021 (vector), Europe, 3-yearly	Copernicus Land Monitoring Service (CLMS) (2021a)	2021	Minimum Mapping Unit (MMU) of 0.25 ha
Urban Atlas Street Tree Layer 2021 (vector), Europe, 3-yearly	Copernicus Land Monitoring Service (CLMS) (2021b)	2021	Minimum Mapping Width (MMW) of 10 m
Vulnerable Infrastructure	Open Street Map Contributors (2026)	2026	Point

Socio-demographic data

To gain insights into the population structure of Olomouc, census 2021 population grid data were downloaded from the Czech Data Portal, providing information on the distribution of women, educational status and unemployment rates at a spatial resolution of 1km. In addition, address points were provided by the Department of Geoinformatics of Palacký University Olomouc under the supervision of Jaroslav Burian. This dataset offers high resolution insights into population density and spatial distribution of vulnerable groups such as children and the elderly. Since the aforementioned population datasets are based on permanent residency and do not consider population mobility, dynamic daytime and nighttime population grid data developed by Rypl et al. (2026) at a spatial resolution of 100m was additionally used.

Table 4 Overview of socio-demographic datasets used in this study.

Dataset	Source	Temporal Resolution	Spatial Resolution
2021 Census, Population Grid	Czech Data Portal (2026b)	2021	1km
Address Points	Department of Geoinformatics, Palacký University Olomouc	2025	Point
Population Grid Daytime and Nighttime	Rypl et al. (2026)	2021	100m

3.3 Software

ArcGIS Pro

ArcGIS Pro (Version 3.5.4) was used to preprocess the available data sources and prepare them as indicators for the UHI risk assessment. At the same time, the UHI risk model was conceptualized and applied. The corresponding results were also visualized and analyzed using simple statistical methods.

ArcGIS Online

ArcGIS Online was used to host relevant feature layers and applications, where corresponding web maps were created with Map Viewer. **ArcGIS Dashboards** was used to create a risk explorer with filtering functionalities and dynamically changing metrics. **ArcGIS StoryMaps** was used to visualize relevant results for decision-makers and the public engagingly. **ArcGIS Experience Builder** was used to link the different applications and to give a layer overview.

RStudio

RStudio was used to clean the temperature measurements of the sensor network and calculate relevant metrics for the summer period of 2025. It was also used to understand the correlation between indicators and how they drive UHI risk. Lastly, UHI hazard was validated and compared to sensor measurements. The corresponding results were visualized using **ggplot2**.

QGIS

QGIS (Version 3.34.11) was used to query OSM data on vulnerable infrastructure. For that, the QuickOSM plugin was utilized to filter relevant facilities for children and the elderly, with the layer extent being the city boundary.

AppEEARS

AppEEARS was used to query LST data and quality control layers from ECOSTRESS, where the starting and end dates as well as the processing area were defined.

Google Colab

Google Colab was used to clean the table on health service providers in Olomouc from the National Register of Health Service Providers and to bring them into a format that allows easy integration as a point layer in ArcGIS Pro.

Microsoft Excel

Microsoft Excel (Version 2606) was used to identify representative LST scenes for the hazard component. It was also used to calculate statistics and to visualize tables using conditional formatting.

3.4 Methods & Processing Procedure

This thesis is structured into a thorough literature review, data preprocessing, UHI risk assessment, visualization and analysis of UHI risk as well as the integration of the results into a web mapping application (Figure 2). Based on the literature review, this study is focused on a UHI risk assessment approach linked to the definitions of the IPCC as well as guidelines of the *Vulnerability Sourcebook* (GIZ, 2014) and the *Risk Supplement to the Vulnerability Sourcebook* (GIZ and EURAC, 2017).

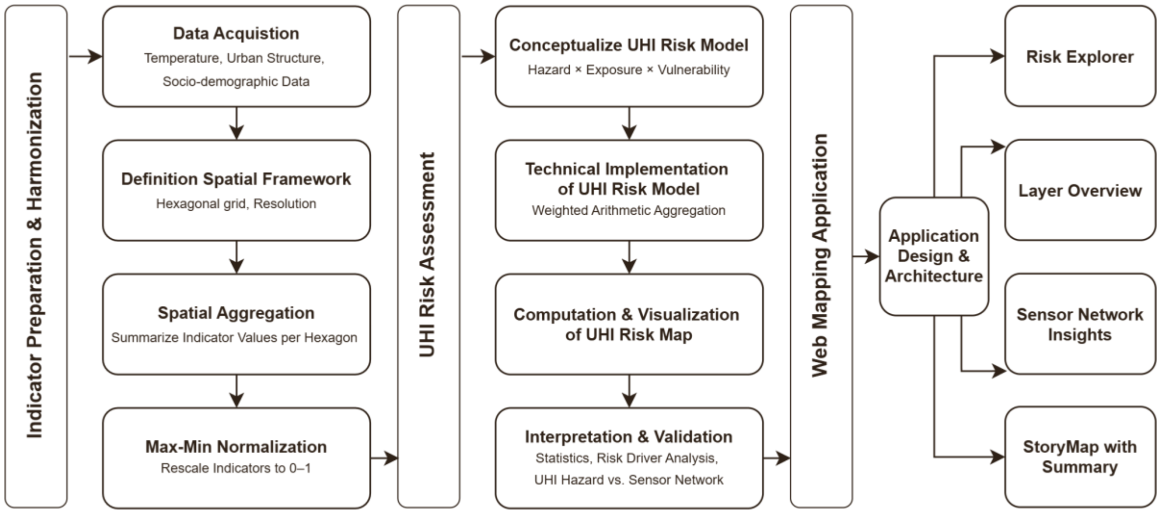

Figure 2 Workflow of this study.

The data collection phase is conducted based on commonly mentioned indicators in the literature (Ellena et al., 2023; Reinwald et al., 2024; Thanvisitthpon, 2023) and consultation with experts from the Departments of Geoinformatics and Geography of Palacký University Olomouc. This is followed by the definition of a spatial framework using a hexagonal grid, which considers the different spatial resolutions mentioned in the data section. Each dataset is then preprocessed to relevant indicators by summarizing its values for each hexagon cell, whereby the exact methodology can vary based on the individual input characteristics. Afterwards, each indicator is normalized using a min-max approach to create coherent and comparable indicators (GIZ, 2014; Räsänen et al., 2019). This phase also includes the preprocessing of the sensor network data, which could not be integrated as an indicator due to the small number of weather stations and is therefore instead used for UHI risk validation.

The second phase includes the UHI risk assessment, where the first step is to conceptualize the UHI risk model and to create a transferable script. For the technical implementation, each indicator was categorized into one of the four components hazard, exposure, sensitivity and adaptive capacity based on expert knowledge and similar studies (Bhattacharjee et al., 2019; Sidiqui et al., 2022; Vaňo et al., 2025). After computing UHI risk and its components, the results are visualized as static maps. Moreover, UHI risk is interpreted statistically and indicators are analyzed according to their contribution to final risk. In this context, the hazard component of UHI risk is also compared to the sensor network measurements to gain additional insights into the thermal patterns in the city.

Lastly, the final web mapping application is created with the four components risk explorer, layer overview, sensor network insights and summary, which are all linked in an engaging experience. The application thereby helps to further explore the results of the UHI risk assessment and to make relevant decisions towards risk adaptation and mitigation.

4 INDICATOR PREPARATION AND HARMONIZATION

The first part of the thesis can be structured into preprocessing and indicator harmonization. This part of the thesis was mostly conducted in ArcGIS Pro. In this context, all datasets are prepared to act as indicators for the UHI risk assessment. This chapter gives an overview of the conducted steps to ensure reproducibility.

4.1 Spatial Framework

To ensure accurate results, this study follows a consistent projection using the Czech national coordinate system S-JTSK Krovak EastNorth (EPSG: 4156). As stated in the literature, choosing a spatial framework with an appropriate scale and spatial resolution is crucial in risk assessment and can lead to different results (Räsänen et al., 2019). While many studies use administrative boundaries, these can be too coarse and do not represent the real distribution of natural phenomena and climate-related hazards. Therefore, for this study, a hexagonal grid was created using *Generate Tessellation,* which was then clipped to the administrative boundary of Olomouc. While different resolutions were tried, the final assessment is conducted using hexagons where each side is 100m long, resulting in an area size of approximately 10,000m² per hexagon. This spatial resolution coincides with many of the initial datasets. At the same time, this hexagon size was chosen since the study area is relatively large and a finer hexagon size would have led to computational issues. The final hexagon grid consists of 10,859 hexagons that build the base for each indicator that is processed. As mentioned below, the hexagons including the lake in the northern part of the study area had to be excluded from the final risk assessment as they would influence the distribution of UHIs in urban areas, especially during the night.

4.2 Indicator Preparation

In general, the preprocessing of each indicator follows a similar approach where *Summarize Within* is used to aggregate the data of each indicator per hexagon. Due to different data structures, this general approach had to be adapted slightly for several indicators as implied below.

4.2.1 Temperature Data

To identify thermal patterns in the study area, land surface temperature data from ECOSTRESS and participatory mapping results from the campaign in Olomouc in 2020 were preprocessed. At the same time, temperature measurements from the sensor network of Olomouc were analyzed to give additional insights into the final UHI risk.

Land Surface Temperature

Land Surface Temperature from ECOSTRESS (ECO_L2_LSTE.002) was acquired for the summer period 2025 (25.06.2025-30.09.2025) via NASA AppEEARS. Under consideration of the statistics table, 15 representative scenes, 5 for daytime and 10 for nighttime, were selected, all of which were without clouds.

Table 5. Selected ECOSTRESS scenes. Scenes marked with * cover daytime.

Scene ID	Date (Local Time)	Average (°C)
ECO_L2_LSTE_002_LST_doy2025176032427_aid0001	25.06.2025 05:24:27	14.58
ECO_L2_LSTE_002_LST_doy2025178050111_aid0001	27.06.2025 07:01:11	14.63
ECO_L2_LSTE_002_LST_doy2025180014709_aid0001	29.06.2025 03:47:09	13.8
ECO_L2_LSTE_002_LST_doy2025181041151_aid0001	30.06.2025 06:11:51	15.73
ECO_L2_LSTE_002_LST_doy2025182032315_aid0001	01.07.2025 05:23:15	12.7
ECO_L2_LSTE_002_LST_doy2025183005756_aid0001	02.07.2025 02:57:56	13.42
ECO_L2_LSTE_002_LST_doy2025220115355_aid0001	08.08.2025 13:53:55*	34.36
ECO_L2_LSTE_002_LST_doy2025223110414_aid0001	11.08.2025 13:04:14*	33.95
ECO_L2_LSTE_002_LST_doy2025224101512_aid0001	12.08.2025 12:15:12*	34.49
ECO_L2_LSTE_002_LST_doy2025226101450_aid0001	14.08.2025 12:14:50*	38.28
ECO_L2_LSTE_002_LST_doy2025227092614_aid0001	15.08.2025 11:26:14*	38.13
ECO_L2_LSTE_002_LST_doy2025236034711_aid0001	24.08.2025 05:47:11	5.58
ECO_L2_LSTE_002_LST_doy2025238052345_aid0001	26.08.2025 07:23:45	8.52
ECO_L2_LSTE_002_LST_doy2025242034612_aid0001	30.08.2025 05:46:12	10.71
ECO_L2_LSTE_002_LST_doy2025250234155_aid0001	08.09.2025 01:41:55	9.24

In ArcGIS Pro, *Raster Calculator* was used for each scene to apply the scaling factor and to transform the temperature values from Kelvin into Celsius using the following formula:

$$LST = (S \times 0.02) - 273.1 \quad (1)$$

where LST is the land surface temperature (°C), S is the original ECOSTRESS scene pixel value and 0.02 is the scaling factor provided with the ECOSTRESS product. Following, the five daytime scenes were compiled into one raster using Cell Statistics, where the mean of the five scenes for each pixel was calculated. The same step was repeated for the ten nighttime scenes, resulting in one LST dataset for the day and one for the night. To identify UHIs in the study area, urban heat island intensity (UHII) was calculated, which can be defined with the following formula (Stewart & Oke, 2012):

$$UHII_i = LST_i - LST_{LCZ\ D} \quad (2)$$

where $UHII_i$ is the urban heat island intensity of pixel i, LST_i is the land surface temperature of pixel i, and $LST_{LCZ\ D}$ is the land surface temperature of the rural reference LCZ D (Low plants) class. The reference temperature of LCZ D was calculated by selecting and exporting class 14 (LCZ D) of the LCZ dataset of Olomouc. With *Extract by Mask*, only the aggregated LST values for day and night inside the LCZ D mask were selected. In *Raster Calculator*, the mean values of the extracted datasets were then used as the reference values to calculate UHII for day and night, where $LST_{LCZ\ D}$ at night was 11.43°C and 36.47°C during the day.

Since the nocturnal UHII layer is strongly influenced by the lake area in the northern part of the city, which would lead to the lake being the most dominant UHI in the study area, these pixels had to be excluded as was done in similar studies (Lauwaet et al., 2024). To do so, a water mask was created using *Raster Calculator*, where pixels exceeding a value of 3 at night were assigned the value 1. The threshold was here defined through visual inspection, with the lake being the only area in the study area with nighttime UHII values larger than 3°C. Pixels of the nighttime UHII layer outside of the water mask were then extracted using *Extract by Mask.*

Following, to aggregate UHII during day and night inside the hexagonal grid, *Zonal statistics as table* was used to calculate the mean value of each hexagon. These results were then joined to the original hexagon layer, where daytime and nighttime UHI were normalized following the general min-max approach.

Participatory Mapping Results

The raw participatory mapping results consist of 1,423 polygons and 668 point features that include thermal comfort and discomfort in a single dataset. Therefore, the first step was to filter the data based on the initial question of the respondents to mark locations where they feel comfortable or uncomfortable on hot summer days. Following, the polygon dataset and point dataset on filtered thermal discomfort were used to calculate the Reported Thermal Discomfort Score (RTDS) introduced by (Lehnert et al., 2021). This method reassigns the weights between points and polygons to reduce overrepresentation of certain locations that can occur when respondents draw uncomfortable areas (see Figure 3). RTDS can be expressed with the following formula:

$$RTDS_i = (P_i \times 3) + G_i + \sum (N_i \times 0.666) \tag{3}$$

where $RTDS_i$ represents the Reported Thermal Discomfort Score for hexagon i, P_i is the number of participatory mapping points within the hexagon, G_i is the number of participatory mapping polygons intersecting the hexagon and N_i represents neighboring hexagons of a hexagon with a point count greater than or equal to one. The neighboring contribution is weighted by a factor of 0.666 and summed across all adjacent hexagons.

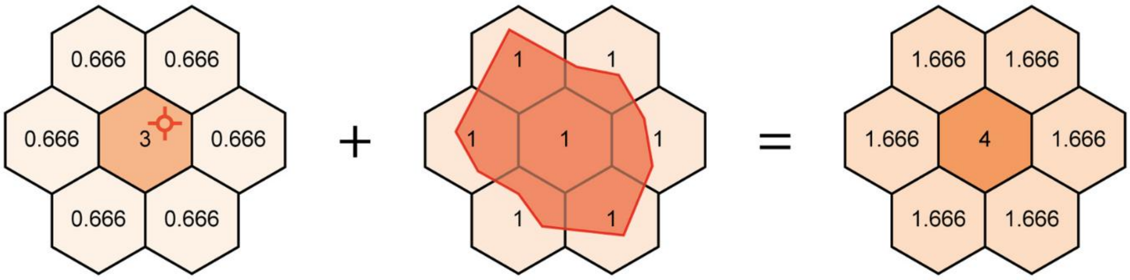

Figure 3 RTDS/RTCS calculation in a hexagonal grid (Lehnert et al., 2021).

To calculate RTDS in ArcGIS Pro, first *Summarize Within* was used twice to identify the polygon count intersecting with each hexagon and the count of points per hexagon. For the latter, *Field Calculator* was used to weigh the point counts more strongly by multiplying them by three as suggested. To account for spatial influence from neighboring hexagons, the *Polygon Neighbors* tool was used to identify adjacent hexagons. The resulting neighbor table was joined with the summarized point counts to identify hexagons with a point count greater than or equal to one. For each neighboring hexagon, an additional neighboring score was calculated as the point count multiplied by 0.666. Since one hexagon can have up to six neighboring hexagons, these neighboring scores were aggregated using *Summary Statistics* to obtain a total neighboring score for each hexagon. Finally, the RTDS was calculated with *Field Calculator* by combining the three components weighted point count, polygon count and the aggregated neighboring score. The same methodology was used to calculate RTCS using the filtered data on thermal comfort.

Air Temperature

Air temperature data were acquired from the sensor network in Olomouc consisting of 10 weather stations. Temperature data at different heights, air pressure as well as wind speed measurements at 15 min intervals were downloaded via the official data portal as CSV files. Due to the vast number of measurements and API limits, the data were downloaded from June 2025 to September 2025 for each month separately. At the same time, temperature from the Czech Hydrometeorological Institute (CHMI) weather station Olomouc Holice was acquired for the same time period as daily aggregations to serve as a reference to calculate UHII using the sensor network measurements.

In RStudio, the sensor network measurements were imported, merged into a single dataset and cleaned by removing duplicates. To ensure comparability across stations, the dataset was transformed from a long to a wide table format so that each timestamp contains all relevant meteorological variables per station. As an additional thermal variable that represents the by humans perceived outdoor temperature, apparent temperature was calculated following the Australian Bureau of Meteorology formula (Steadman, 1994):

$$AT = T_a + 0.33e - 0.70WS - 4 \tag{4}$$

where T_a represents an air temperature measurement, e equals vapour pressure and WS is wind speed. Vapour pressure was derived from relative humidity using the following formula:

$$e = \frac{RH}{100} \times 6.105 \times \exp(\frac{17.27 \times T_a}{237.7 + T_a}) \tag{5}$$

where T_a represents an air temperature measurement and RH equals relative humidity. To characterize thermal conditions at a daily interval, the 15-minute observations were aggregated per station into summary statistics including air temperature and apparent temperature values. At the same time, UHII was calculated as the daily temperature difference between each station and the rural reference of Olomouc Holice, where UHII was identified under mean, maximum, and minimum temperatures, with the latter representing nighttime UHII. These daily statistics were then further aggregated and additional seasonal thermal indices were computed for each station for the whole summer period of 2025 (Table 6).

Table 6 Computed thermal indices for each station for the summer period of 2025.

Metric	Definition	Unit
Air Temperature (T)	Mean, maximum, minimum air temperature	°C
Apparent Temperature (AT)	Mean and maximum apparent temperature	°C
Diurnal Temperature Range (DTR)	Mean, maximum and minimum DTR (Tx-Tn)	°C
Urban Heat Island Intensity (UHII)	Mean and maximum UHII during day and night	°C
Summer Days (SD)	Days with Tx ≥ 25°C	Days
Hot Days (HD)	Days with Tx ≥ 30°C	Days
Warm Nights (WN)	Nights with Tn ≥ 17 °C	Days
Heat Waves (HW)	At least three consecutive days with maximum temperature ≥30 °C	Days

Finally, these metrics were used to visualize spatial and structural differences in thermal exposure through a series of plots. At the same time, the station coordinates were added to the final dataset to export and upload to ArcGIS Online. There, the dataset provides additional insights to improve spatial interpretation of urban heat exposure.

4.2.2 Urban Structure

Urban Atlas Land Cover/Land Use 2021

The Urban Atlas Land Cover/Land Use 2021 vector layer was reclassified in *Field Calculator* using the code field to assign subjective values ranging from 0 (low UHI risk) to 1 (high UHI risk). For instance, green urban areas (*Code: 14110, 14120, 14130*) and forests (*Code: 31000*) have been given a value of 0, indicating no risk. On the other hand, the highest risk was given to continuous urban fabric (*Code: 11100*) due to high soil sealing and a large number of (vulnerable) people living in these areas. The full reclassification scheme for all 20 classes present in the study area is shown in Table 7.

Table 7 Reclassification of Urban Atlas classes (0 = low risk, 1 = high risk).

Value	Classes
1.00 – 0.80	Continuous urban fabric >80% (11100, 1.00); Industrial, commercial, public, military and private units (12100, 0.90); Discontinuous dense urban fabric 50–80% (11210, 0.85); Fast transit roads and associated land (12210, 0.80)
0.75 – 0.60	Other roads and associated land (12220, 0.75); Airports (12400, 0.65); Discontinuous medium density urban fabric 30–50% (11220, 0.65); Railways and associated land (12230, 0.60)
0.50 – 0.35	Mineral extraction and dump sites (13100, 0.50); Construction sites (13300, 0.50); Discontinuous low density urban fabric 10–30% (11230, 0.45); Isolated structures (11300, 0.35)
0.30 – 0.20	Land without current use (13400, 0.30); Discontinuous very low density urban fabric <10% (11240, 0.25); Sports and leisure facilities (14200, 0.20)
0.05	Arable land (21000); Pastures (23000)
0.00	Green urban areas – public/private/unknown access (14110, 14120, 14130); Forests (31000); Herbaceous vegetation associations (32000); Water (50000)

Instead of assigning the value of the largest overlapping Urban Atlas class to each hexagon, an area-weighted approach was chosen, as this method better represents the heterogeneous urban structure within each hexagon by accounting for the proportional contribution of all intersecting land-use classes. This approach can be summarized as:

$$UA_i = \frac{\sum(C_j \times A_j)}{A_i} \tag{6}$$

where UA_i represents the weighted Urban Atlas value for hexagon i, C_j is the reclassified Urban Atlas class value of the intersected polygon j, A_j represents the area of the intersected polygon within the hexagon and A_i is the total area of the hexagon i.

In ArcGIS Pro, *Intersect* was first used between the hexagon grid and the reclassified Urban Atlas layer, resulting in segmented polygons for each Urban Atlas class within every hexagon. Using *Field Calculator*, a weighted value was calculated by multiplying the reclassified Urban Atlas value by the corresponding intersected polygon area. Next, *Summary Statistics* was applied to aggregate the weighted values for each hexagon based on the *GRID_ID* of the hexagons. The summarized values were then joined back to the original hexagon grid. Finally, the total weighted value was divided by the total area of each hexagon using the *Field Calculator*, resulting in an area-weighted mean Urban Atlas value for each hexagon.

Urban Atlas Street Tree Layer 2021

The Urban Atlas Street Tree Layer 2021 is a vector layer showing rows or patches of trees within the cityscape, thereby giving important insights into urban green in Olomouc. With *Summarize Within*, the polygon layer was summarized inside the initial hexagon grid. For this layer, it was important to use a valuable shape unit (km²) to understand how much area of each hexagon is covered by urban green, where a high coverage of urban green later indicates a high capacity to reduce vulnerability.

Vulnerable infrastructure

Vulnerable infrastructure consists of OSM point data on schools, kindergartens, senior homes as well as hospitals. The OSM data were acquired using QGIS and the

QuickOSM tool. In ArcGIS Pro, *Summarize Within* was then used to understand the count of vulnerable infrastructure points in each hexagon.

Practitioners

The data on practitioners and pharmacies was downloaded from the National Registry of Health Service Providers as a CSV table with all entries until March 2026. To correctly load the table in ArcGIS Pro, the CSV file was preprocessed in Google Colab by adding the columns Lat and Lon with the corresponding data from the GPS field.

Following, points were created in ArcGIS Pro using the adapted table with the Lat and Lon attributes as input coordinates. Since the table shows practitioners of all kinds that might not necessarily contribute to adaptive capacity in the context of UHIs, the data were filtered. In this context, only pharmacies and practitioners related to primary care, emergency and acute care as well as with a focus on vulnerable groups, meaning children and the elderly were kept. As suggested in the literature, a buffer with a 100 m distance was created around the remaining points. Subsequently, *Summarize Within* was used to calculate the number of polygons containing a relevant practitioner within a 100m distance per hexagon.

4.2.3 Socio-Demographic Data

Population density

Population density was calculated from the daytime and nighttime population grid provided by the Department of Geoinformatics. The data is available in 100m raster cells, which is why the dataset for the day and night distribution was converted to polygons. Following, these newly created polygons were used to summarize the total count of the population at day and night per hexagon using *Summarize Within*. This led to two individual indicators for the final risk assessment, one for population density during the day and one at night.

Children & Elderly

Children under the age of 14 and the elderly over the age of 65 have been selected as vulnerable groups in the context of this study. For both groups, the point features of the address points acted as the input datasets. With *Summarize Within*, two separate layers were created containing the total count of children and the elderly per hexagon.

Women, Unemployment & Low Education

To further identify vulnerable groups, the Census 2021 Population Grid with a spatial resolution of 1km was used. For this, data on the distribution of women, unemployed persons and people with primary education or lower were chosen. Due to the low spatial resolution, the population data were redistributed following a dasymetric methodology using the address points as input. To do so, the first step was to identify the number of address points per census grid cell using *Summarize Within*.

After that, for the first indicator, a new attribute was created via *Field Calculator* that divides the count of women in a grid cell by the number of address points. This results in the distribution of women per address point inside a certain grid cell. To distribute these counts back to the actual address points, *Spatial Join* was used with address points as the target feature. Here, address points within a grid cell were given the corresponding value. Lastly, following the general methodology, *Summarize Within* was used with the hexagon grid and address points as input to calculate the redistributed total count of women per hexagon. These steps were repeated for unemployment and low education, resulting in three individual indicators giving insights into vulnerable groups.

4.3 Indicator Harmonization

All indicators follow the same spatial framework, meaning that they have all been aggregated inside the hexagon grid of 100m, which results in 10,859 hexagons per indicator. Since all indicators have different value ranges and different units, it is important to normalize them into unitless values on a common scale ranging from 0 to 1. This also gives the values valuable meaning since values close to 0 represent a low risk, while those close to 1 show a high risk (GIZ, 2014). For metric values, which most of the indicators in this study can be associated with, this normalization can be done using the min-max method with the following formula:

$$X_{i,0-1} = \frac{X_i - X_{Min}}{X_{Max} - X_{Min}} \tag{7}$$

where X_i represents the individual data point to be transformed, X_{Min} is the minimum value observed for the indicator, X_{Max} is the maximum value observed for the indicator, and $X_{i,0-1}$ represents the normalized value scaled to a range between 0 and 1.

To do this in GIS, the maximum and minimum values for each indicator were acquired using the *Explore Statistics* tool, whereby most indicators show a minimum value of 0, which simplifies the formula. Subsequently, the normalized values for each indicator were calculated in *Field Calculator* using the corresponding maximum and minimum values. The only exception is the Urban Atlas layer, where the initial dataset was nominal and has been subjectively reclassified into a range from 0 to 1, which is why min-max normalization doesn't have to be applied here. For each indicator, this leaves one normalized column, which will be the input for the risk assessment.

To avoid redundancy and overrepresentation of socio-demographic groups, the indicators children, elderly, women, unemployed persons and people with primary education or lower have been summarized into one indicator called vulnerable populations before the final risk assessment. After normalizing each of the indicators mentioned individually, their values have been summed and divided by the number of indicators for each hexagon in *Field Calculator*.

To simplify the risk assessment methodology, the indicators need to be summarized in a single dataset, which was achieved using *Join Field* with the initial hexagon layer as the input table. To ensure that only the relevant columns are joined, *field mapping* was used for each indicator, resulting in a single dataset containing the normalized values for each indicator in separate columns. For the visualization in the final web mapping application, next to the normalized indicator values, selected absolute counts have been joined to the final layer, mainly regarding the number of vulnerable people, practitioners or urban green per hexagon.

5 UHI RISK ASSESSMENT

In general, the risk assessment follows the definition of the AR5 of the IPCC. While most studies use individual and slightly adapted definitions, indicators and equations, this study aims to use a standardized approach, which was introduced as the *Vulnerability Sourcebook* by the GIZ (GIZ, 2014) and is supplemented by the *Risk Supplement to the Vulnerability Sourcebook* (GIZ and EURAC, 2017).

5.1 Conceptual Framework of the UHI Risk Model

The UHI risk model was created with the aim of making the methodology easily reproducible, transferable and scalable across study areas, especially considering advanced data availability in Olomouc in the near future. First, the components hazard, exposure, sensitivity and adaptive capacity are calculated individually using *weighted arithmetic aggregation*. This means that individual indicators are multiplied by their weights, summed and lastly divided by the sum of their weights, as indicated in the following formula:

$$CI = \frac{(I_1 \, * \, w_1 + I_2 \, * \, w_2 \, + \, \ldots \, I_n \, * \, w_n)}{\sum_1^n w} \tag{8}$$

where CI represents a composite indicator that can either be hazard, exposure, sensitivity or adaptive capacity, I is an individual indicator inside the specific component and w is its corresponding weight.

Secondly, vulnerability is calculated separately before the final risk is computed. To do so, the component adaptive capacity needs to be inverted since a high adaptive capacity represents a lower risk, which does not comply with the general principle of low values indicating low risk and vice versa. Therefore, the adaptive capacity values are subtracted from one. While the GIZ recommends summing the indicators of sensitivity and inverted adaptive capacity, this approach led to an overestimation of vulnerability in areas with zero sensitivity and very low adaptive capacity. To address this issue, the GIZ approach was slightly adapted by operationalizing vulnerability through the following multiplicative formula, which is modified from Voelkel et al. (2018):

$$V = S \cdot (1 - AC) \tag{9}$$

where V represents vulnerability, S sensitivity and AC adaptive capacity, while the latter is inverted immediately using this formula. In this way, adaptive capacity acts as a modifying factor that can reduce existing sensitivity rather than generating vulnerability on its own, thereby reducing the influence of adaptive capacity in areas where sensitivity is absent or very low.

Lastly, the final risk is computed by using *weighted arithmetic aggregation*, similar to the calculation of composite indicators. Hence, the three components hazard, exposure and vulnerability are combined and divided by the sum of their weights as follows:

$$R = \frac{(H * w_H) + (V \, * \, w_V) + (E \, * \, w_E)}{w_H + w_V + w_E} \tag{10}$$

where R is the final risk, H represents hazard with w_H being its corresponding weight, V vulnerability with w_V as its weight and E exposure with w_E as its weight.

5.2 Technical implementation

The UHI risk model was implemented as a custom script tool within an ArcGIS Pro toolbox (*.atbx*), making the entire workflow executable through a graphical user interface without requiring users to interact with the underlying code directly. The script is written in Python and relies on the ArcPy library that provides access to geoprocessing tools and data access functions within the ArcGIS environment. The toolbox is available on GitHub at this link (https://github.com/annabellekiefer/UHI_Risk_Assessment).

Before writing the script, the tool parameters were configured in the toolbox properties. These include an input and output layer as well as *Value Table* parameters for the risk components, binding each indicator directly to its corresponding weight in a single row-based input. These parameters were set as dependent on the input layer to automatically populate available field options from the chosen input layer. At the same time, optional weights for the final components hazard, exposure and vulnerability were configured. During execution, the script processes each hexagon individually, calculates the weighted component scores, derives vulnerability and risk and writes the results as new columns to the output layer. NULL values, which mostly occur at the study area boundary, are managed by excluding them from the calculation and redistributing their weights among the remaining valid indicators, preventing data gaps from distorting component scores.

Regarding the weights of the individual indicators as well as risk components, the model uses equal weights of one as the default, which can be individually adjusted. Similarly, the model gives users the opportunity to individually place indicators inside the risk components since this classification of indicators varies across the literature and is dependent on the specific requirements of a study. As an output, the model adds the columns hazard, exposure, sensitivity, adaptive capacity, vulnerability and risk to the output layer, giving users the ability to visualize components individually.

5.3 Computation UHI Risk Map

Using the graphical user interface of the script tool, the harmonized hexagonal layer was set as the input layer. Following, each indicator was manually placed into the components hazard, exposure, sensitivity and adaptive capacity. This classification mainly follows standard approaches in the literature, whereby the placement of the indicators thermal comfort and discomfort has proven challenging since this dataset has not been included in UHI risk assessment before. In consultation with experts from the department, it was decided to place thermal discomfort into sensitivity since it shows how susceptible residents already are to heat-related harm. On the other hand, thermal comfort is seen as an existing buffer against heat stress that typically coincides with green infrastructure, which is why it was included in adaptive capacity. The remaining indicators were classified as follows.

Table 8 Classification of indicators into risk components.

Component	Indicators
Hazard	UHII Day, UHII Night
Exposure	Urban Structure, Population Density Day & Night
Sensitivity	Vulnerable Population, Vulnerable Infrastructure, Reported Thermal Discomfort Score (RTDS)
Adaptive Capacity	Practitioners, Urban Green, Reported Thermal Comfort Score (RTCS)

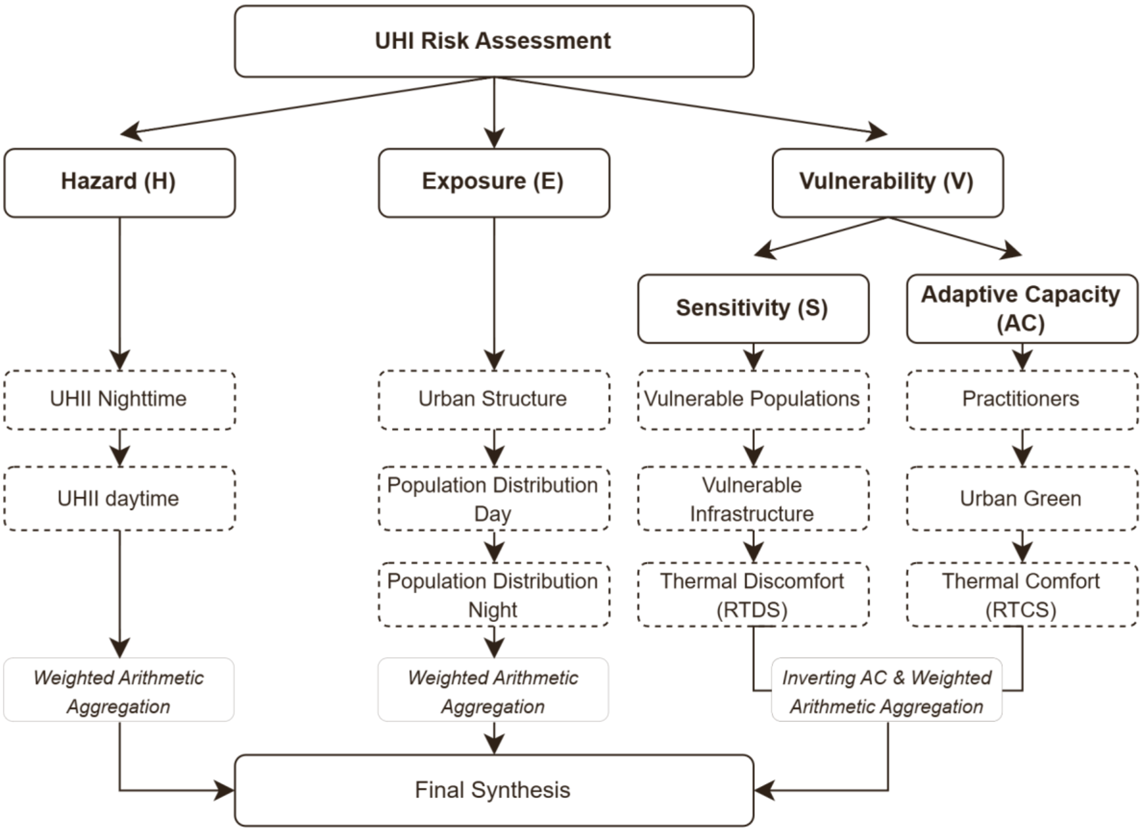

Figure 4 Calculation of UHI risk based on indicators for hazard, exposure and vulnerability.

For the weights of the indicators and components, the default equal weights were taken. After running the script, each component as well as the final risk index were visualized individually using five classes and natural breaks (Jenks) as the classification method. This classification coincides with existing literature and works well with the different value ranges of the risk components.

In this context, a sequential color scheme ranging from light orange to dark red (Figure 5) was chosen where the highest color intensity represents the highest risk. This color palette coincides with the natural association of red being perceived as risk or danger. To ensure consistency, this color scheme was applied to risk, its components and all indicators. For the indicators of the adaptive capacity component, this means that dark red here represents a high ability to reduce vulnerability.

Figure 5 Color scheme used in this study.

5.4 Risk Model Analysis and Validation

To analyze the final risk map statistically, to understand how different indicators drive UHI risk and to understand similarities and disparities between UHI risk and especially hazard compared to sensor network data, custom scripts were created and run in RStudio. The two scripts, structured according to the sub-goals of this chapter can be found in the appendix as part of the digital medium. At the same time, basic statistics were calculated in ArcGIS Pro by aggregating UHI risk into microzones as a second spatial unit.

5.4.1 Statistical Characterization and Risk Driver Analysis

To understand key statistics of UHI and its components as well as to identify which indicators most strongly shape the final risk score, the output of the UHI risk model with all indicators, components and risk values was exported as a CSV from ArcGIS Pro and imported into RStudio. For each of the eleven normalized indicators, descriptive statistics were calculated, including mean, standard deviation, median and interquartile range, thereby giving insights into both the central tendency and spatial coverage of each indicator. The same statistics were subsequently calculated for the composite components hazard, exposure, sensitivity, adaptive capacity, vulnerability and risk, allowing a direct comparison of how broadly each component is expressed across the study area.

Spearman correlation, which is based on ranks and thereby assesses whether one variable increases, the other one also tends to increase, was used to identify which indicators most strongly drive the final risk score. The same procedure was repeated for the five composite components against the final risk score, thereby evaluating whether each component contributes proportionally to the overall result. In this context, a Spearman correlation matrix was calculated between all indicators, as well as an extended matrix additionally including the composite components and the final risk score. Indicator pairs exceeding an absolute correlation coefficient of 0.80 were highlighted since they can show potential redundancy between indicators. Nonetheless, for the UHI risk assessment, even indicators with a high correlation coefficient can give crucial insights into a few hexagons. The correlation results were visualized as bar charts showing the strength and significance of each indicator's and component's relationship with risk, complemented by correlation heatmaps highlighting redundancy across the indicator set and strong dependencies between indicators and components.

5.4.2 Validation and Interpretation UHI Risk

To validate the final UHI risk map and compare the hazard component to the sensor network measurements, the hexagons intersecting with one of the ten weather stations were selected and exported as a new layer. This layer was then imported into R and linked to the station-based observations and seasonal thermal indices for summer 2025, enabling a station-to-hexagon comparison between observed thermal conditions and modelled spatial risk representations.

The relationship between observed and modelled variables was assessed using Spearman correlation. Particular attention was given to nighttime conditions, as these represent the most dominant UHIs, for example by examining the relationship between hazard and sensor-derived nighttime UHI intensity. Key thermal metrics were then visualized as scatterplots or correlation heatmaps, thereby highlighting important differences between observed and modelled thermal patterns.

Since the current sensor network of ten stations is too small to be integrated directly as an indicator into the UHI risk model, this comparison instead serves to assess whether air temperature measurements capture information beyond what the hazard component already represents. As the network is planned to be expanded across a wider range of LCZs, this validation step was designed to determine whether such an expansion would be a worthwhile basis for future integration of air temperature metrics into the hazard component.

6 WEB MAPPING APPLICATION

The web mapping application acts as an effective tool to visualize the results of the UHI risk assessment. With the target group defined as decision-makers, the results are communicated in an interactive and understandable way. In this context, the focus lies on the identification of efficiently identifying UHI risk areas that need to be prioritized when applying mitigation strategies.

6.1 Application Design and Architecture

The final web mapping application was created in ArcGIS Experience Builder due to prior experience with similar use cases and the possibility to efficiently integrate layers hosted on ArcGIS Online. To enhance the overall user experience, ArcGIS Dashboards was additionally used to include relevant dashboard elements. Similarly, ArcGIS StoryMaps was used to communicate the results of the UHI risk assessment engagingly. In this context, ArcGIS Experience Builder serves as the primary application where the external dashboard and story elements are embedded.

The design and usability are focused on the target group of decision-makers. Special emphasis is placed on the integration of easily understandable functionalities, complemented by information buttons to provide further instructions and insights. Similarly, an introduction window is included in the experience, so that users are immediately acquainted with the objectives of the study. At the same time, the web mapping application orients itself on existing web applications of the department of geoinformatics, especially connected to the EnCLOD project that is closely linked to this study. This ensures efficient cross-use of multiple related applications. Furthermore, the feedback of several experts was included in the final web mapping application, which further ensures user-friendly design.

Since the web mapping application serves different goals of interactively exploring UHI risk and communicating the results, four independent components, namely risk explorer, layer overview, sensor network and summary, have been created and linked with each other through the header section of the experience. At the same time, a help section was included as a fifth component that is linked to the introduction screen and header section, allowing users to access instructions on how to use the different components. For the first three components, individual web maps have been created with Map Viewer, mainly displaying the final risk hexagon layer and the sensor network data containing ten weather stations with thermal insights into the summer period of 2025.

In this context, Map Viewer was used to style and classify the hexagon layer, where a similar approach as for the static risk maps was applied. At the same time, a minimalistic base map was selected, the visibility range of the layer was defined and a blending mode was chosen for the hexagon layer. Finally, for both the hexagon as well as sensor network layer, pop-ups were enabled and restructured for effective integration into the final experience.

6.2 Risk Explorer

The main functionality of the risk explorer is the ability to filter risk and its components hazard, exposure and vulnerability in the final hexagon layer. To do so, four separate number selectors have been configured in the sidebar, which are all displayed as a slider for the value range of the corresponding component. After expert-based user testing, additional textual information was provided on the description of risk and its components as well as on explaining how the value ranges can be classified from low to high. The filters are linked to the main map and indicators so that the content automatically changes as soon as one or several filters are applied. To regain the initial map view, users also have the possibility to reset the filters.

Next to filtering the data, the lasso tool has been added as an additional selection tool in the map view, which enables users to draw an area on the map that they are interested in. In this context, layer actions have been applied to the indicators and chart, which are therefore automatically updated with the selection of a study area. At the same time, pop-ups have been enabled on the map when a hexagon is clicked, providing the user with additional insights on UHI risk components and their indicators.

The aforementioned indicators are visualized on the right side of the dashboard and give insights into key metrics that drive UHI risk. For most indicators, the sum was chosen to display the relevant absolute count, while for the nighttime UHII the average is shown. Next to a title, each indicator has an information button that explains the relevance to the final risk. To show the distribution of risk and its components, an additional serial chart was configured with the average risk, hazard, exposure and vulnerability values. Similar to the indicators, this chart is automatically updated with changes in the map extent or through the application of filters.

6.3 Layer Overview

The layer overview enables users to compare layers and gain insights into the structure of the different components and underlying indicators. Due to the large number of layers, a grouping structure was implemented in Map Viewer with one layer group for risk and its components and another one for the initial indicators. In this context, the final hexagon layer was duplicated, dragged into the corresponding layer group and styled by choosing the attribute of the component or indicator. In the properties, exclusive visibility was enabled to improve the usability of the final map. Instead of having to turn each layer on and off manually, users can now select one layer per group.

In ArcGIS Experience Builder, the layer overview page was configured with a map view on the right and a sidebar with the map layers and legend on the left. To switch between map layers and legend, a views navigation has been configured. For the main functionality of this component, a swipe widget was configured, where risk and its components were selected as leading layers and the 11 indicators as trailing layers. The swipe tool was set to be activated by default and a description on how to use the tool was provided at the top of the map layers panel. Since users should solely focus on the swipe tool, additional functionalities such as popups have been disabled to avoid visual clutter.

6.4 Sensor Network Insights

This page view is connected to the sensor network data, where decision-makers get additional insights into the distribution of thermal patterns in the city center. The corresponding map was created in Map Viewer and focuses on the 10 weather stations in Olomouc, which were styled and accompanied by labels. In addition, the final hexagon layer is visualized as a secondary dataset through increased transparency.

In ArcGIS Experience Builder, the page was designed in a similar way as the layer overview with a map view on the right and a sidebar on the left. The sidebar here shows two different charts that give insights into the thermal characteristics of the stations. After expert feedback, an additional description of the sensor network was added in the sidebar. At the same time, a views navigation was added to switch between the two charts.

The first column chart displays mean and maximum UHII during daytime as well as nighttime UHII, while the second chart focuses on the number of hot days and warm nights per station. After adding a title, legend and appropriate color scheme, the charts were configured in a way that enables users to select the data of a weather station in the chart. This then automatically highlights the corresponding weather station on the map. By clicking on the point of a weather station, users can gain additional insights into the thermal behavior based on pop-up content. In the map view, users also have the possibility to switch layers on and off and to inspect the legend.

6.5 StoryMap as Summary

The StoryMap shows a summary of the results of the UHI risk assessment and is thereby the final part of the web mapping application. To fit into the design of the web mapping application, a custom design theme was created and applied. The summary is communicated through basic text elements, data visualizations and interactive features such as swipe and a map tour. The most important insights are highlighted as quotes to create emphasis. A navigation bar was added at the top, which structures the StoryMap into introduction, risk framework, final risk map, priority areas, sensor network and conclusion.

While the introduction, risk framework and final risk map mainly include text elements and static maps, one of the main features of the StoryMap is the map tour on priority zones. Here, users are guided through neighborhoods with high UHI risk, where individual strategies on UHI adaptation and mitigation are proposed for each zone. Following, the sensor network section consists of text elements and charts that explain the importance of integrating this data source into the UHI risk assessment in the future, while the conclusion identifies the most important key takeaways for decision-makers.

7 RESULTS

This chapter introduces the main results of this thesis, maintaining the structure of the practical part. In this context, the final indicators, components and UHI risk are presented. To view the resulting maps in high resolution, a map gallery was set up as part of the thesis website, which can be found at this link (https://www.geoinformatics.upol.cz/dprace/magisterske/kiefer26/gallery.html). In addition, the results of the final web mapping application for decision-makers are presented here and can be accessed via this link (https://experience.arcgis.com/experience/bd0cb55005cf4592a6a077444d34ed48).

7.1 Indicator Preparation and Harmonization

All eleven indicators follow the same spatial framework of 100m spatial resolution that results in 10,859 hexagons per layer. Due to the max-min normalization of all indicators and the creation of a standardized unit and value range, they can be compared to each other by applying basic descriptive statistics. It becomes clear that UHI intensity acquired from ECOSTRESS LST is the most dominant phenomenon in the study area, with a mean value of 0.5 during the day and 0.54 at night, indicating high spatial coverage (Table 9). This also becomes evident through visual interpretation where UHII values exceed zero in almost the entire boundary of the city (Figure 6).

Urban structure also has high spatial coverage and is dominant in most of the city, with a mean of 0.29. Interestingly, this indicator has the highest standard deviation (0.35) of all indicators, indicating a strong spatial contrast between the city center and the more rural outskirts. The relatively low median of 0.05 (Table 9) confirms a lower spatial coverage, where the mean score is driven by high-risk hexagons in the city center, whereas urban structure is less dominant in the outskirts of Olomouc.

Table 9 Descriptive Statistics of the UHI risk indicators.

Indicator	Component	Mean	Median	SD
UHII Day	Hazard	0.50	0.53	0.21
UHII Night	Hazard	0.54	0.54	0.15
Urban Structure	Exposure	0.29	0.05	0.35
Day Population	Exposure	0.00	0.00	0.02
Night Population	Exposure	0.01	0.00	0.04
Vulnerable Population	Sensitivity	0.01	0.00	0.05
Vulnerable Infrastructure	Sensitivity	0.00	0.00	0.03
RTDS	Sensitivity	0.01	0.00	0.03
RTCS	Adaptive Capacity	0.01	0.00	0.05
Urban Green (AC)	Adaptive Capacity	0.04	0.00	0.12
Practitioners (AC)	Adaptive Capacity	0.00	0.00	0.04

It becomes clear that the other indicators are strongly localized and only occur in a few hexagons, while most of the study area is not influenced by them. Because of this, most mean and median values remain close to zero. Urban green here shows a relatively high standard deviation of 0.12 (Table 9), which can be traced back to a higher concentration of urban green in the city center compared to the outskirts of the city.

Nonetheless, these localized indicators still highlight important spatial distributions of their specific phenomenon. In this context, especially the indicators for population density and the distribution of vulnerable groups show important delineations in urban areas close to the city center. Vulnerable infrastructure here shows the lowest spatial coverage, where only a limited number of hexagons exceed zero values. Similar to the indicator highlighting the number of practitioners per hexagon, these indicators still provide crucial insights in a few relevant hexagons, which is why their integration into the final UHI risk model is valuable.

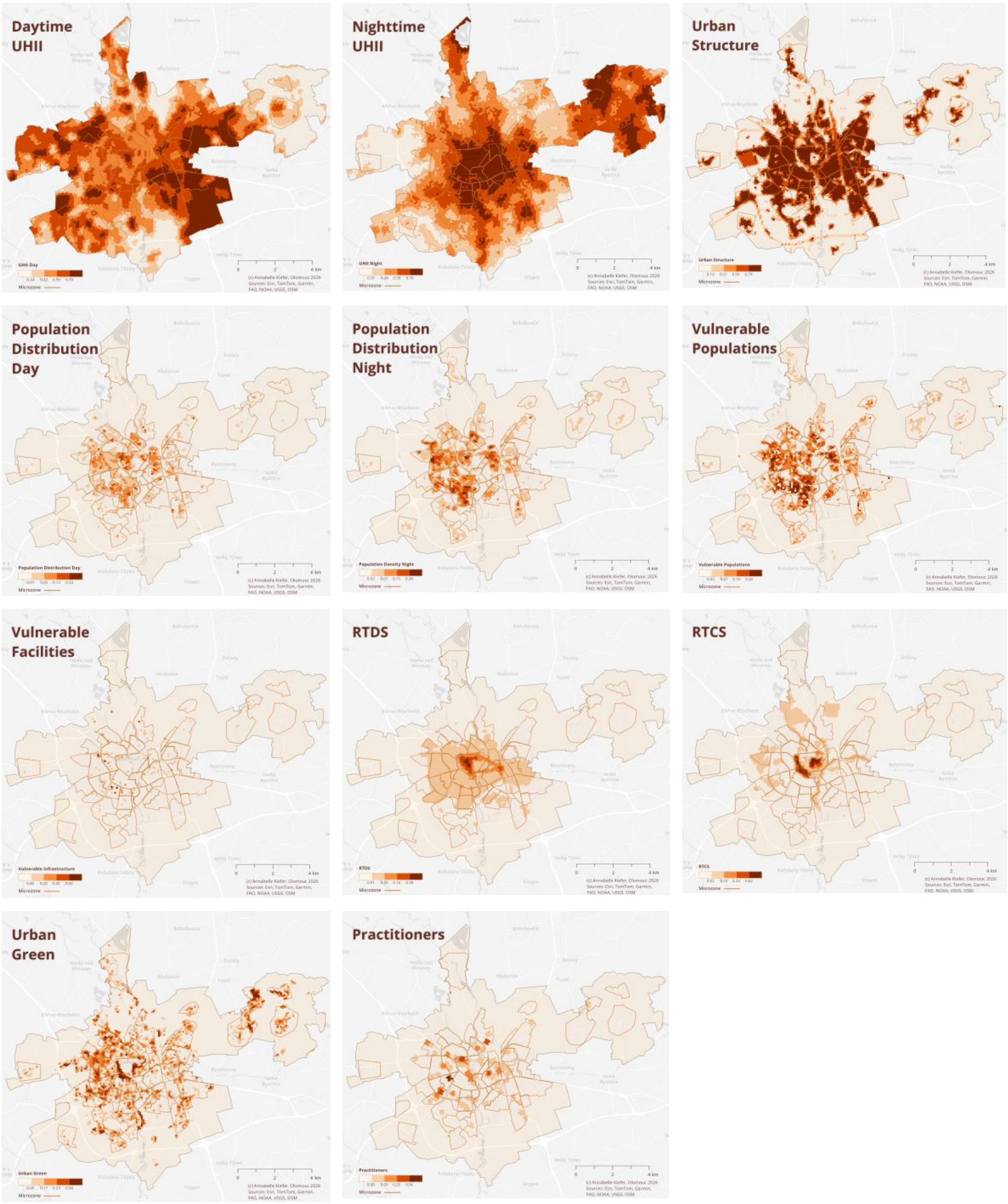

Figure 6 Indicator maps contributing to final UHI risk.
Higher-resolution versions are available in the Map Gallery.

By visually inspecting the different indicator maps, similar spatial patterns between indicators can already be detected, which is why strong correlations can be assumed. In this context, especially the two population density indicators for day and night distribution as well as the vulnerable population indicator show similar patterns in urban areas. This is confirmed by a high Spearman correlation of 0.88 between daytime and nighttime population density (Figure 7). Due to crucial differences in a relevant number of hexagons, it still made sense to integrate both layers into the final UHI risk assessment despite their high overall correlation. Similarly, the correlation between vulnerable populations and population distribution is high at 0.76 during the day and 0.79 during the night (Figure 7), which can be traced back to similar input datasets based on permanent residency and strong linkages between population density and the distribution of vulnerable groups.

The high correlations between urban structure and population indicators as well as thermal discomfort show that most people live in the densest urban areas where they also feel most uncomfortable in summer. Interestingly, a weak negative correlation was found between UHII during day and night (-0.12), suggesting that surfaces which heat up strongly during the day, such as bare soil, are not necessarily retaining this heat at night, where densely built-up areas become more relevant.

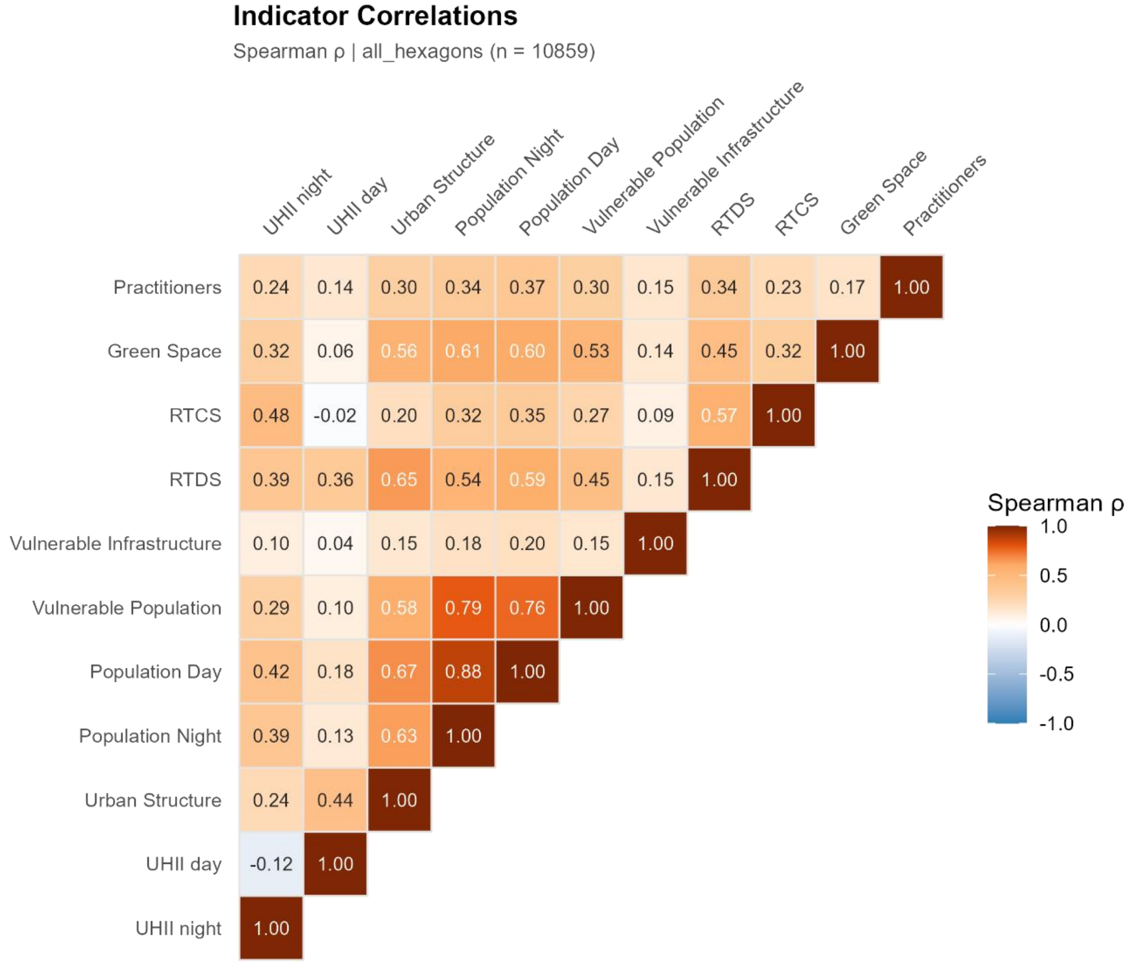

Figure 7 Spearman correlations between indicators used in this study.

7.2 UHI Risk Assessment

For the UHI risk assessment, the first step was to calculate the corresponding components hazard, exposure, sensitivity and adaptive capacity, which will be presented below. These results are followed by the final risk map based on the components.

7.2.1 Component Maps

Comparing the different component maps, it becomes evident that hazard is the most dominant component with values exceeding zero in almost the whole study area (Figure 8). In contrast, exposure is more centered around urban areas and thereby shows similarities to urban structure. The spatial coverage of sensitivity is even less profound and is mostly restricted to populated areas, with high values being found in the old town and surrounding neighborhoods (Figure 8). Adaptive capacity is spread slightly further across the study area, with the strongest concentration in the public parks of Olomouc that increase thermal comfort and the ability to cope with UHI risk.

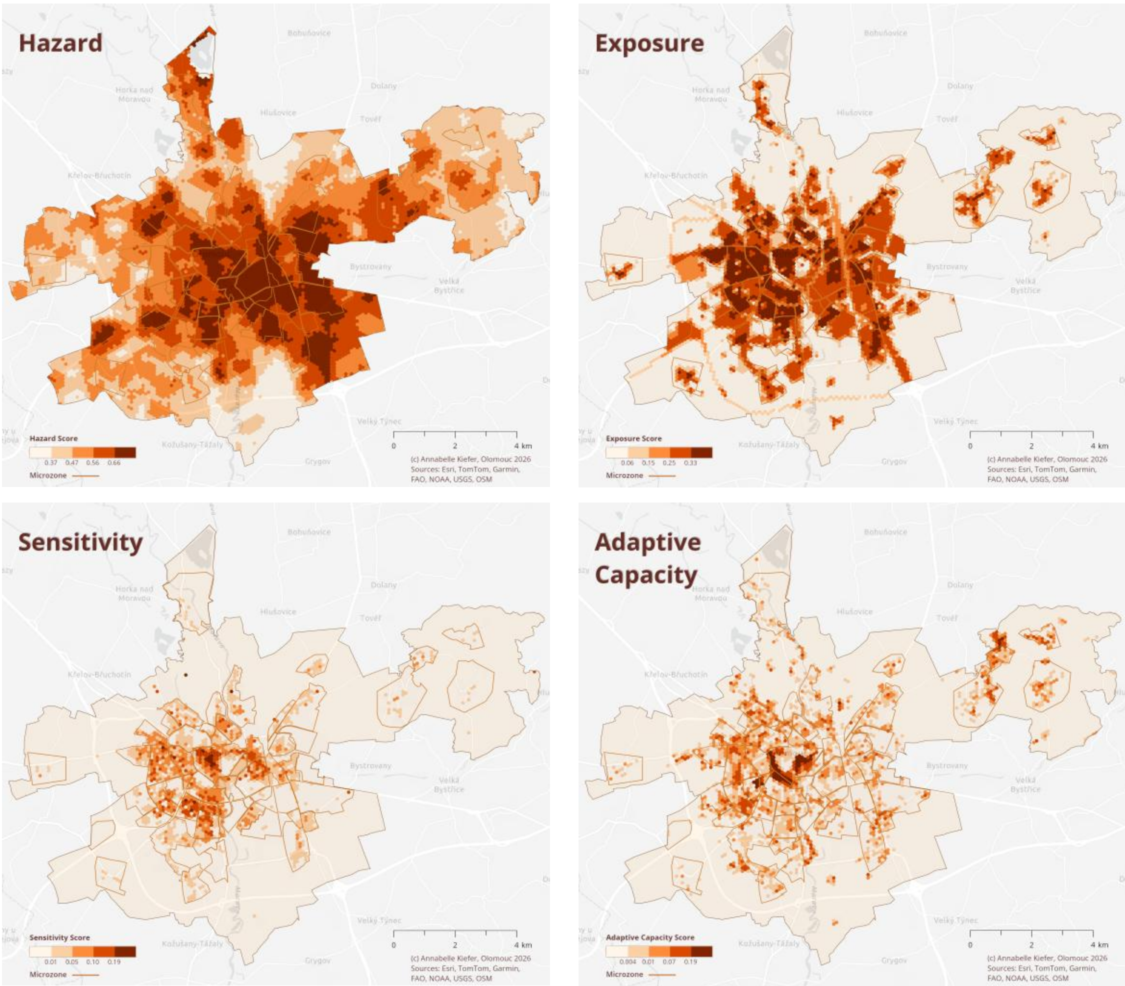

Figure 8 Component maps contributing to final UHI risk.
Higher-resolution versions are available in the Map Gallery.

Through visual inspection, it becomes clear that some components are influenced by certain indicators, whereas other indicators seem to have less influence. In this context, the highest correlation can be found between exposure and urban structure with 0.99 (Table 10), whereas the two population indicators included in exposure show lower correlations (population day: 0.71; population night: 0.70). This can be traced back to the high spatial coverage of urban structure with a spatial contrast between the city center and surrounding rural areas, while the population indicators are mostly aggregated in urban areas. Similarly, RTDS strongly correlates with sensitivity (0.92) as well as RTCS with adaptive capacity (0.78), which is related to the relatively high spatial coverage and strong connections to the other indicators of their components.

In contrast, vulnerable infrastructure has with 0.2 the lowest correlation with its component sensitivity due to its low occurrence in the study area (Table 10), thereby contributing comparatively little to the variability of its component despite being weighted equally in the calculation. Interestingly, high correlations could also be found for indicators and components they were not assigned to, for example between urban structure and sensitivity (0.73). This highlights the spatial co-occurrence and potential redundancy of indicators especially in the city center, with a dense urban fabric and high population, which can also lead to higher reported thermal discomfort.

Table 10 Correlation between indicators and corresponding components.

Indicator	Component	Correlation Value
Urban Structure	Exposure	0.99
RTDS	Sensitivity	0.92
RTCS	Adaptive Capacity	0.78
Daytime UHI	Hazard	0.78
Urban Green	Adaptive Capacity	0.77
Population Day	Exposure	0.71
Vulnerable Populations	Sensitivity	0.68
Population Night	Exposure	0.70
Nighttime UHI	Hazard	0.48
Practitioners	Adaptive Capacity	0.31
Vulnerable Infrastructure	Sensitivity	0.20

7.2.2 UHI Risk

Risk Drivers

Similar to the component maps, the risk map clearly indicates that some indicators drive risk more than others. The spatial pattern of risk especially seems to coincide with urban structure and UHII. Urban structure here has the highest Spearman correlation with 0.81, which corresponds to a high spatial coverage and variance as well as a high correlation with the exposure component. Similarly, thermal discomfort (RTDS) and daytime UHII also both show high correlations (Figure 9). As mentioned earlier, these indicators are often spatially related to more than one indicator and component, which is why they are driving UHI risk more strongly and achieve higher correlation rankings.

On the other hand, indicators of the adaptive capacity component generally score lower correlations, with 0.48 for urban green and 0.32 for the number of practitioners present. This can also be traced back to the adapted formula of calculating UHI vulnerability, where adaptive capacity is only included as a reducing factor. The lowest correlation can be found between risk and vulnerable infrastructure with 0.17 (Figure 9), which coincides with earlier findings and can be explained by the spatial pattern and low spatial coverage of the indicator dataset.

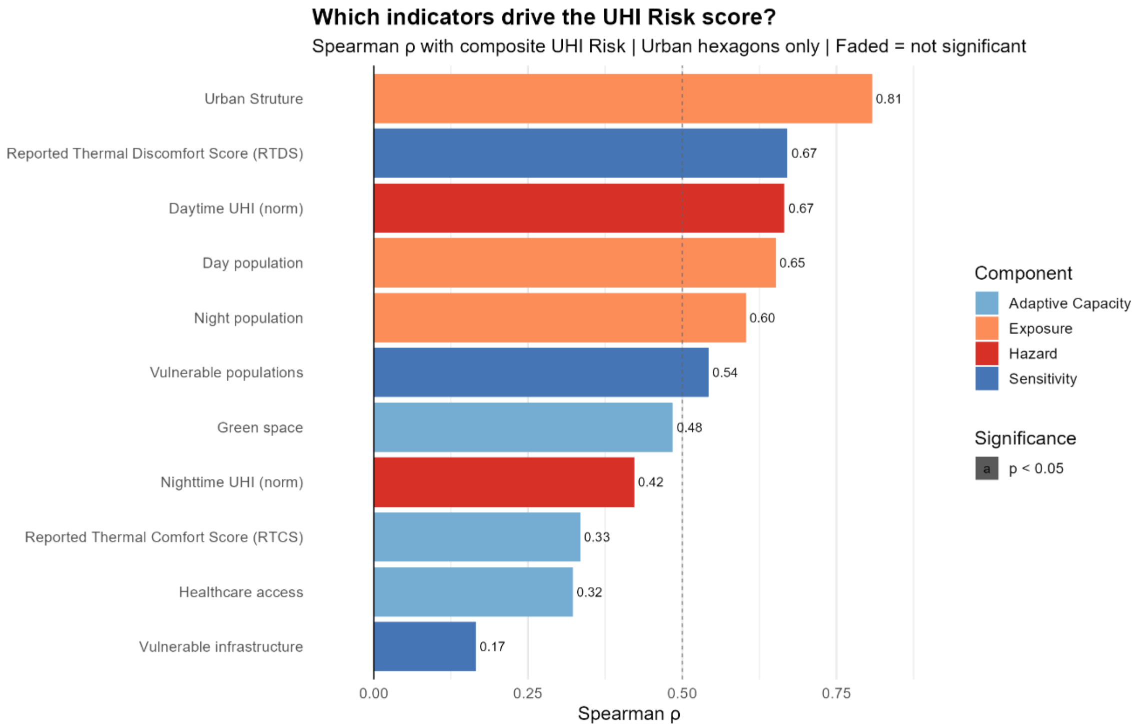

Figure 9 Spearman correlation between indicators and final UHI risk.

Risk Map

The values of the final UHI risk map range from 0 to 0.59 with a mean value of 0.21, where higher risk values can generally be found in urban areas close to the city center, while the outskirts show lower risk. In this context, especially the old town as well as surrounding neighborhoods show higher risk values, whereas the public parks clearly indicate reduced risk (Figure 10). When comparing different microzones that are based on administrative boundaries and adapted to the urban characteristics of an area, the highest risk can be found in Kosmonautů with an average value of 0.35, while Heyrovského (0.34) and Nové Sady sever (0.33) also have high risk values. In contrast, the lowest risk can be found in Topolany with 0.16, which is located at the western edge of the study area (Table 11).

Interestingly, the high risk values of microzones OC Haná and Sladkovského are closely connected to high hazard, with the latter having the lowest vulnerability value of 0.01 (Table 11), indicating that risk in this area is mainly driven by high surface temperatures, whereas vulnerable populations are less present. The high UHI risk of Kosmonautů is also connected to increased hazard values, while there is also a higher vulnerability than in the industrial zones mentioned before, indicating that this microzone combines commercial with residential areas. On the other hand, microzones Heyrovského and Nové Sady sever have the highest vulnerability values, indicating the presence of a high number of vulnerable groups (Table 11). For the city center, risk is especially combined through high hazard (0.64) and high vulnerability (0.07). This again underlines the importance of including different components into UHI risk, since hazard alone might lead to an overrepresentation of built-up areas with high LST, where sensitive populations do not necessarily have to be present, while exposure and vulnerability include exactly these missing indicators.

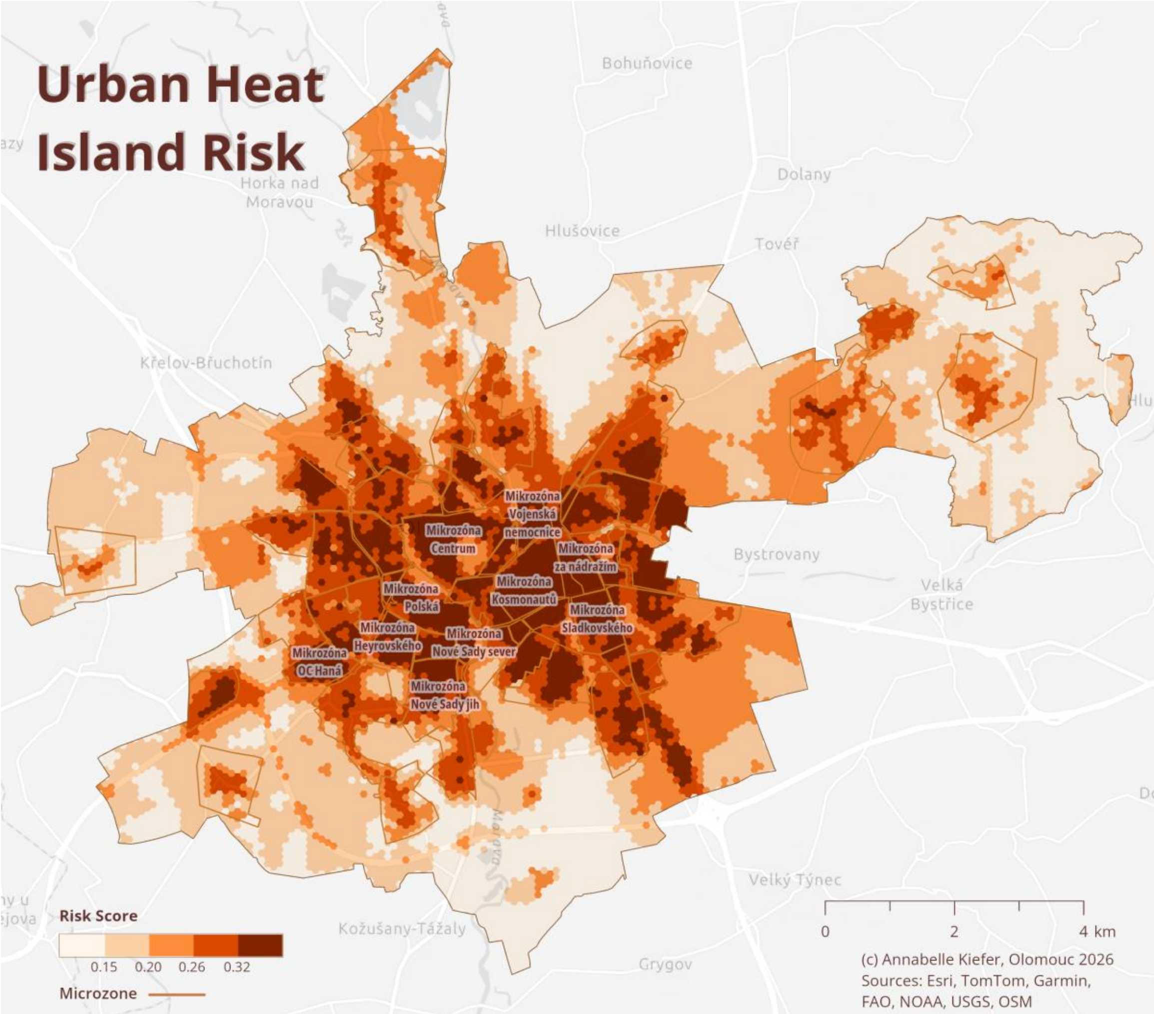

Figure 10 Final UHI risk map.

Table 11 Microzones with the highest UHI risk and corresponding component values.

Microzone	Mean Risk	Mean Hazard	Mean Exposure	Mean Vulnerability
Kosmonautů	0.346	0.698	0.296	0.044
Heyrovského	0.336	0.602	0.320	0.087
Nové Sady sever	0.329	0.583	0.318	0.085
Vojenská nemocnice	0.324	0.591	0.320	0.060
Nové Sady jih	0.323	0.614	0.297	0.058
Centrum	0.321	0.641	0.253	0.068
Sladkovského	0.313	0.666	0.266	0.006
za nádražím	0.311	0.625	0.272	0.035
OC Haná	0.307	0.628	0.271	0.020
Polská	0.306	0.656	0.277	0.046

Priority Zones

From the final UHI risk maps and their interpretation into microzones and specific neighborhoods, several priority zones can be identified that differ in their distribution of component and indicator values. Therefore, individual recommendations for UHI mitigation and adaptation are necessary. One of these priority zones is the city center with its dense urban structure and high pedestrian activity. Although this area has lower vulnerability values compared to typical residential areas (Table 11), many visitors report thermal discomfort in summer, which is why measures improving thermal comfort should be implemented.

On the other hand, the microzones around Nové Sady & Povel show the highest number of vulnerable populations, increasing overall risk and vulnerability values. Since the residential groups living in these areas include children, the elderly and persons with a lower educational background, who might be less prepared and aware of risks of extreme heat events, early warning systems tailored to the specific needs of the residents are crucial in this context. Another example of increased vulnerability is the senior residence in Chválkovice, a neighborhood that besides the industrial zone in the south shows low risk values (Figure 10). Due to the high concentration of the elderly in the senior residence itself, the risk value is higher compared to its surroundings, indicating that high sensitivity combined with low exposure and hazard can still be seen as a priority location for targeted monitoring during heat wave events.

Lastly, the industrial zones Sladkovského in the east and OC Haná in the west of the city show areas where risk is mainly driven by hazard, while vulnerability and exposure are comparatively low due to a lack of permanent residential population. Therefore, recommendations for UHI measures differ here and focus more on mitigating trickling effects of heat load to adjacent neighborhoods rather than direct improvements of thermal comfort in the area itself. In contrast, Kosmonautů not only consists of commercial buildings that drive the hazard component, but also residential areas leading to increased exposure and vulnerability values (Table 11). Because of this combination, the area needs to be highly prioritized regarding UHI measures, where mitigation strategies have to focus on both the local population itself as well as on the adjacent commercial areas whose increased surface temperatures can negatively influence thermal comfort in the neighborhood.

Table 12 Definition of priority zones for UHI mitigation and adaptation. Image source: Google Maps, accessed 24 July 2026.

Microzone/ Neighborhood		Description	Recommendations
City Center		Dense urban structure, high pedestrian activity, increased thermal discomfort (high RTDS)	Increase of thermal comfort for pedestrians (shading and cooling structures)
Nové Sady & Povel (Polská & Heyrovského)		Dense housing blocks, increased vulnerability values due to a high number of vulnerable populations (children, the elderly, women, low educational background)	Early warning systems tailored to vulnerable populations, social support during extreme heat events
Chválkovice (Senior Citizens' Home POHODA)		Neighborhood with sparse urban structure and a large amount of vegetation, while most of the area has low risk values, high risk is identified for the senior residence due to increased sensitivity	Targeted monitoring and social support during heat wave events
Industrial & Commercial Zones (Kosmonautů, Sladkovského, OC Haná)		Highest hazard values with comparatively low vulnerability values, extensive sealed surfaces and flat rooftops, area largely unoccupied during the night	Reducing surface temperatures to decrease contribution of heat load to adjacent neighborhoods

7.2.3 Validation UHI Risk Map

In the final report of the city of Olomouc on adaptation and mitigation strategies (Adaptační a mitigační strategie města Olomouce - analytická část), one section is dedicated to UHIs and identifying areas at high risk of heat stress. In this context, findings from the project “Identification of locations at risk of heat stress – a tool for sustainable urban planning” provided by the technology agency of the Czech Republic and conducted between 2018 and 2019 were used. One of the outputs of this project is a vulnerability map for Olomouc with a spatial resolution of 30m, which constitutes a synthesis of layers on imperviousness, built-up areas, surface permeability, green cover and predominant forest types. At the same time, fact sheets with proposals for appropriate adaptation measures were given for selected sites at high risk of heat stress (Vizina et al., 2020).

The final map shows the degree of susceptibility to climate change with colors ranging from green (low susceptibility) to red indicating high susceptibility. It becomes clear that the highest level of susceptibility can be found in several industrial zones on the outskirts of the city, whereas the city center and areas close to the railway also show high values. This clearly indicates that this synthesis map is largely influenced by built-up surfaces. While a direct comparison between this vulnerability map and UHI risk analyzed as part of this study is difficult due to varying spatial resolutions, it still becomes clear that additional risk areas could be identified in this study. These are especially tied to residential areas such as Povel and Nové Sady, where a large number of vulnerable populations can be found.

On the other hand, industrial built-up hotspots are less dominant in the UHI risk map of this study, indicating that the current adaptation strategy focuses mostly on hazard and exposure, while vulnerability as a human-centered approach is mostly missing. This underrepresentation of people-centric metrics can also be found in the map of selected locations for UHI adaptation, which mostly shows industrial zones and shopping centers (Vizina et al., 2020). In contrast, the recommendations developed in this study focus more on residential areas with high proportions of children, the elderly, women and people with a lower educational background.

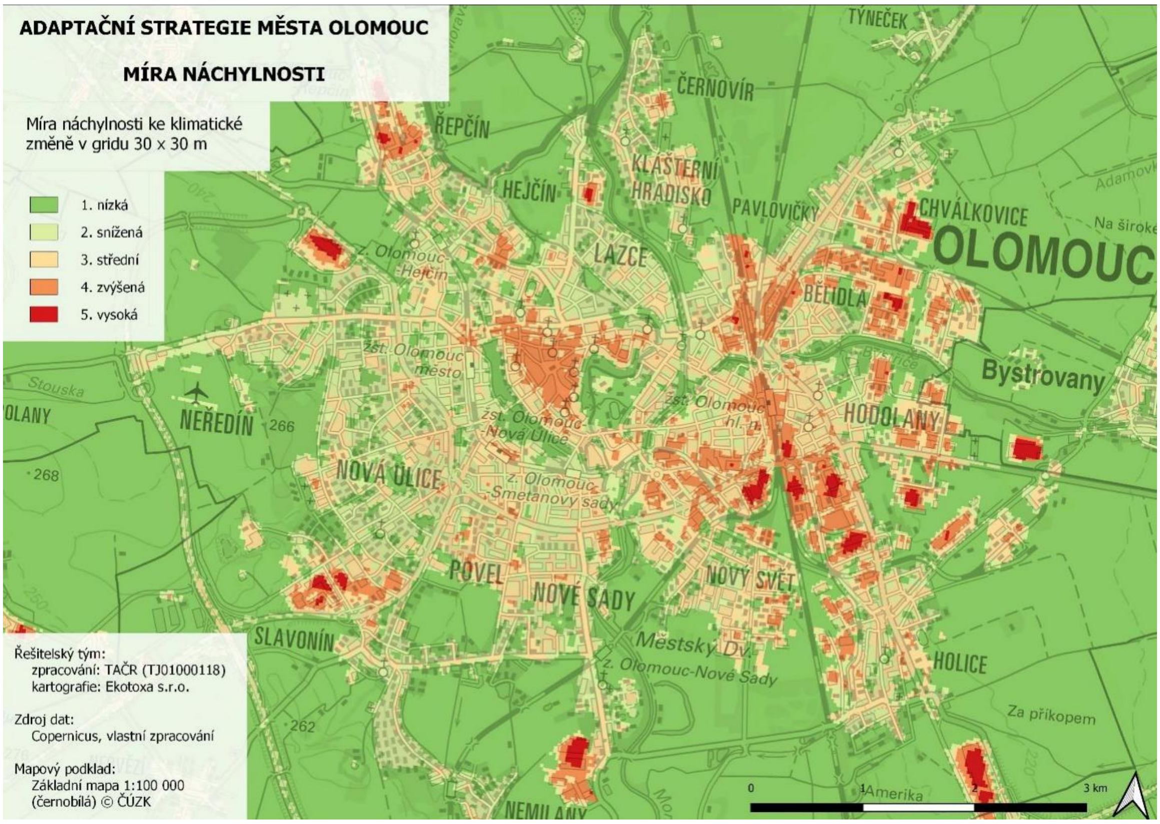

Figure 11 Adaptation Strategy of the City of Olomouc with the degree of Susceptibility to climate change (Vizina et al., 2020).

7.2.4 Sensor Network Data

The processed sensor network data of the ten weather stations for the summer period of 2025 gives crucial insights into microclimatic differences inside the city center. In this context, several thermal indicators were calculated, such as the number of hot days or warm nights. For the latter, the highest number was found in Tržnice with 20 warm nights, which lies at the outskirts of the old town and is classified as bare soil (LCZ 16). Similarly, Trnkova, located inside a residential area and defined as open high-rise, as well as Nádraží, representing the area around the main train station, registered 19 warm nights in lasts year summer period (Figure 12).

Interestingly, Nám. Republiky, which is the only weather station classified inside LCZ 2 (compact midrise), only registered 14 warm nights (Figure 12). Although this weather station is located in the densest urban fabric, its exact location is in an open space including a parking lot and a small fountain, which is why the measurements might be influenced by the cooling effect of blue infrastructure. The lowest number could be found in Smetanovy sady with 12 warm nights, indicating the cooling effect of the public parks of Olomouc that can improve the thermal comfort of residents.

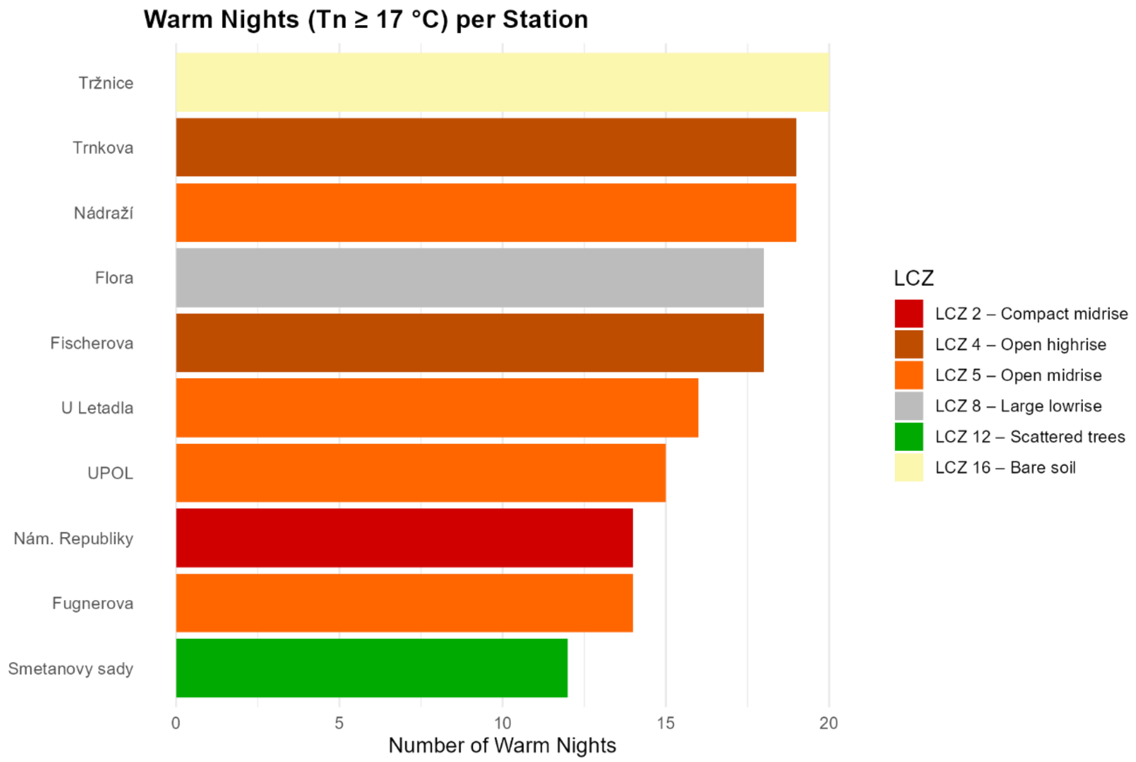

Figure 12 Number of warm nights per sensor weather station.

Since the number of sensors is currently too low to be integrated into the actual UHI risk assessment, the sensor network data were compared to the hazard component of UHI risk. This helps to understand if the data can provide additional insights in the future when more sensors will be available in Olomouc. Particularly interesting is the comparison of UHI hazard with nighttime UHII from the weather stations of the sensor network. In this context, there is only a weak Spearman correlation of 0.1 (Figure 13), illustrating that there is no linear relationship between the two metrics for most stations.

Only for Smetanovy sady weather station, there is some agreement with the lowest nighttime UHII and one of the lowest hazard values, which resonates with its location in a public park of Olomouc that is improving the microclimate. In contrast, Tržnice directly contradicts a relationship between the two metrics, with the highest UHII in connection to only moderate modelled hazard. Similarly, Fugnerova and UPOL show comparatively low or moderate observed UHII despite ranking among the highest modelled hazard values (Figure 13), indicating that the current hazard component does not fully capture thermal patterns related to UHIs.

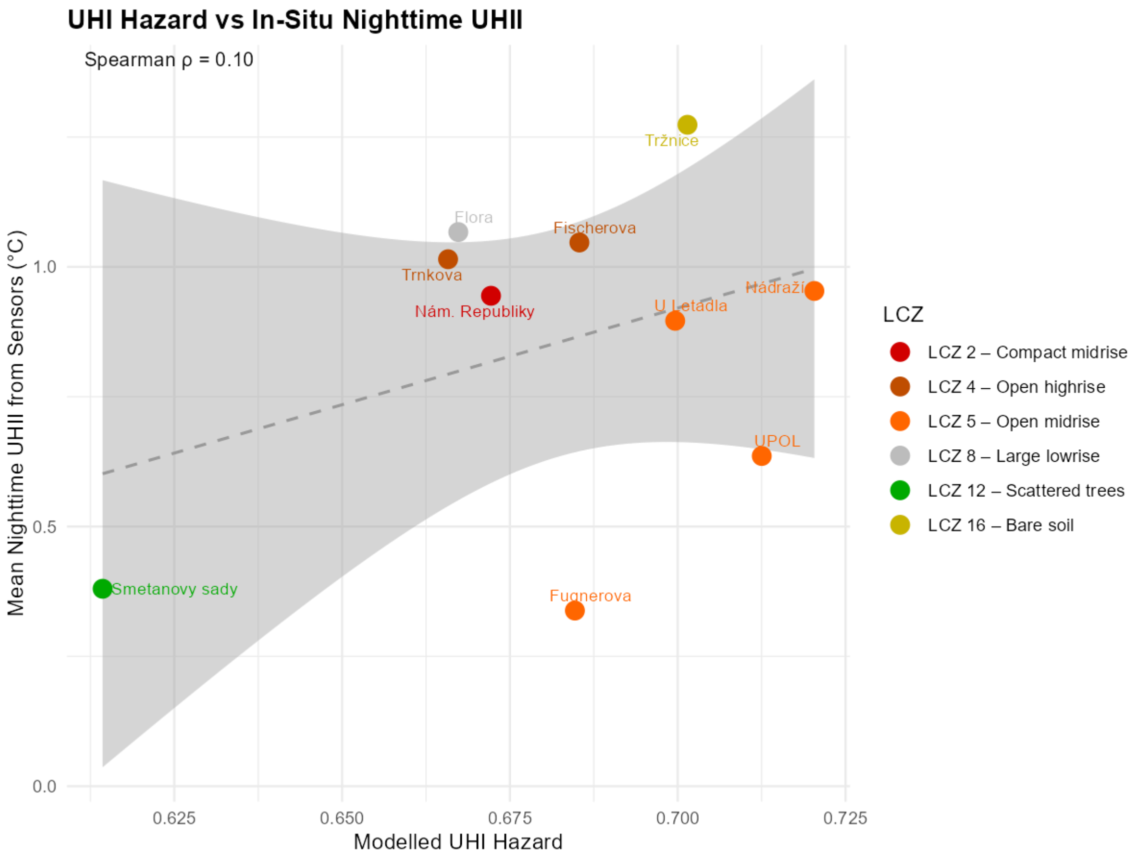

Figure 13 Comparison between UHI hazard and nighttime air temperature UHII.

This can be further investigated by ranking the stations from highest to lowest hazard and thermal metrics acquired from the sensor network data. According to the literature, although the values of air temperature measurements and land surface temperature cannot be directly compared with each other (Voogt & Oke, 2003), there is the assumption that the highest LST values should correspond to the highest air temperatures (Středová et al., 2021).

This assumption applies to Smetanovy sady weather station, where low rankings for hazard correspond to low nighttime UHII measured with sensors and a low number of warm nights. In contrast, there is low agreement between air temperature and LST for other stations such as UPOL, where hazard and nighttime UHII acquired from LST are high compared to lower air temperature metrics (Table 13).

This becomes even clearer for Trnkova, which shows clear indications for nocturnal UHIs with 19 warm nights and a relatively high nighttime UHII acquired from temperature data, whereas the hazard is low, not least due to the lowest UHII at night computed from LST (Table 13). Since Trnkova is located in a residential area with a large number of vulnerable populations, these differences between LST and air temperature-acquired metrics indicate that the integration of air temperature measurements could further improve the insights gained from the hazard component.

Table 13 Comparison of different thermal metrics. Shading indicates each station's rank within a metric, from dark red (highest value) to beige (lowest value).

Station	Hazard	UHII Night (LST)	UHII Night (T)	Warm Nights
Fischerova	0.69	1.44	1.05	18
Flora	0.67	1.52	1.07	18
Fugnerova	0.68	1.41	0.34	14
Nádraží	0.72	1.81	0.95	19
Nám. Republiky	0.67	1.78	0.94	14
Smetanovy sady	0.61	1.80	0.38	12
Trnkova	0.67	1.40	1.01	19
Tržnice	0.70	2.01	1.27	20
U Letadla	0.70	1.48	0.90	16
UPOL	0.71	2.08	0.64	15

7.3 Web Mapping Application

The final web mapping application allows decision-makers to thoroughly understand UHI risk at different scales and with its underlying data structure. After reading an introduction screen, users can explore this first component and visualize the final risk layer according to their specific criteria. In this context, one application area is to filter hexagons that contain not only high risk, but also high vulnerability. Applying multiple filters can thereby help to differentiate hexagons that are solely influenced by LST from those where vulnerable populations are present.

This can be accompanied by defining a custom study area, where users gain insights into the distribution of risk and its components as well as relevant metrics. Metrics such as the number of vulnerable populations as well as the availability of green space and general practitioners help decision-makers to differentiate between areas where relevant features to cope with UHI risk are already available versus where there is currently a lack. The latter areas can then be targeted for UHI mitigation and adaptation.

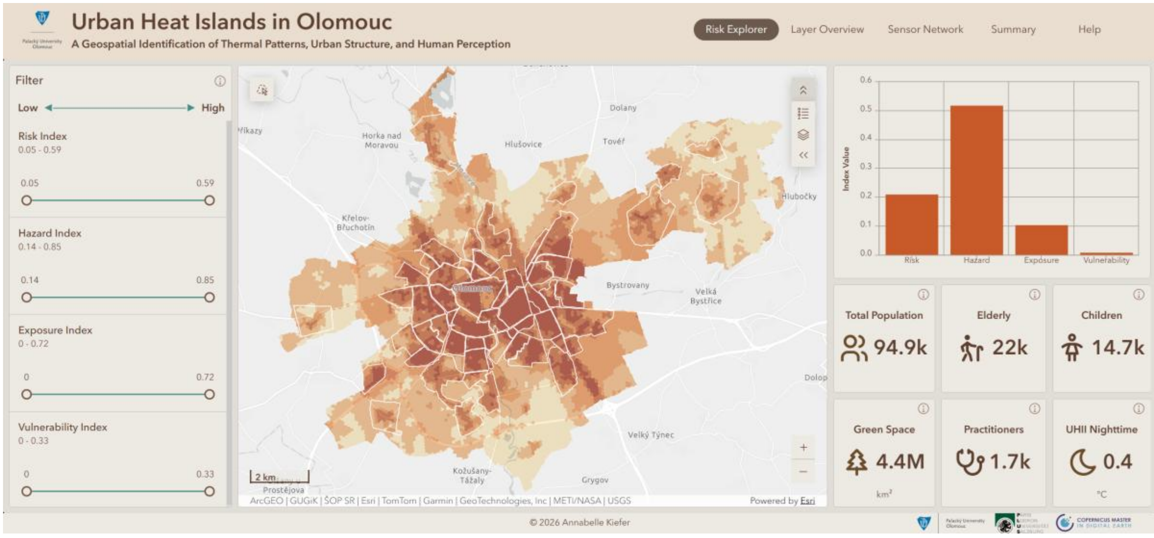

Figure 14 Risk Explorer of the final web mapping application.

The layer overview effectively lets users compare risk and its components with the initial indicators, thereby helping them understand the underlying layer architecture of the final risk map. Users can here compare input layers that are relevant for their specific use case. Additionally, the sensor network component provides additional insights into thermal metrics such as UHII, where users can understand the maximum temperature difference between the urban center and its rural surroundings during day and night in the summer season. This component can be updated in the future, when additional sensors will be available that will offer a thorough understanding of microclimatic differences in the city.

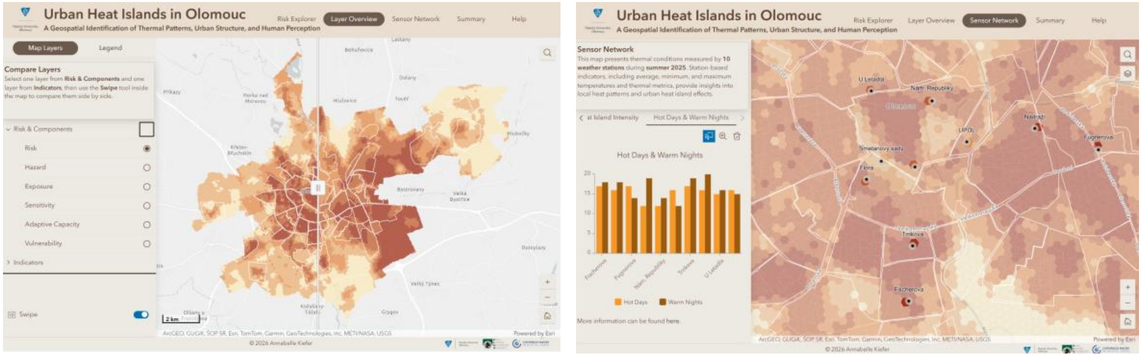

Figure 15 Layer overview (left) and sensor network insights (right) of the final web mapping application.

Lastly, the StoryMap provides a summary of the results of UHI risk, informing and engaging decision-makers. Next to text elements, charts and static maps, dynamic features such as the swipe tool let users compare risk and hazard interactively. This comparison is crucial to understand the advantages of analyzing UHI risk through a combination of hazard, exposure and vulnerability instead of solely focusing on LST or air temperature as has been done in many studies.

Similarly, another crucial part is the map tour where users gain insights into the most affected areas that need to be prioritized regarding UHI mitigation and adaptation. Neighborhoods around the city center, Povel and Nové Sady are highlighted here and differentiated according to their urban structure and population characteristics. In this context, individual recommendations for measures to mitigate UHIs are provided for each priority area based on the initial indicators.

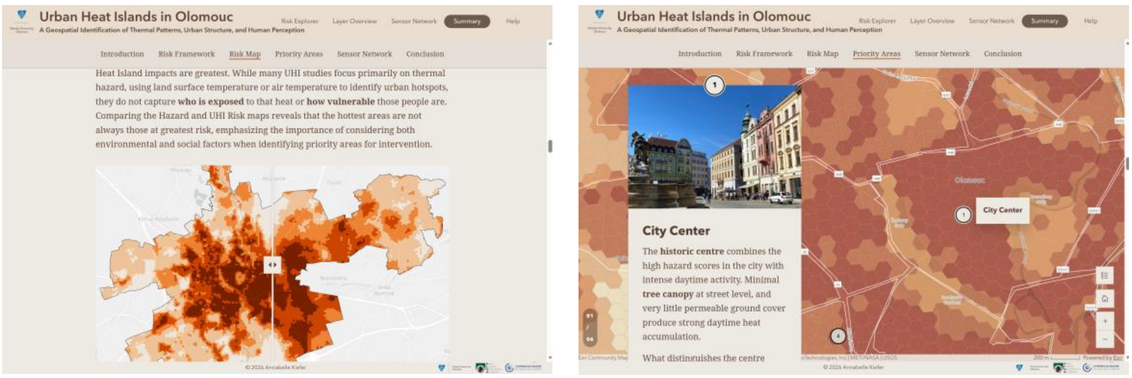

Figure 16 StoryMap of the final web mapping application.

8 DISCUSSION

In this chapter, data limitations and methodological adaptations are discussed. The data and methods used are compared to relevant literature. In this context, an alternative solution is mentioned as future work.

8.1 Indicator Preparation & Harmonization

Spatial Framework

For this study, a hexagonal grid was chosen as the spatial framework to conduct the UHI risk assessment. The advantage here is that this approach is not reliant on arbitrary boundaries, gaining insights into UHI risk for particular neighborhoods instead of having to focus on city boundaries. While summarizing UHI risk in Olomouc to identify the microzones with the highest risk, it became clear that important insights on the distribution of UHI risk can get lost due to varying area sizes. Although microzones are already adapted to include real urban conditions, especially for the microzones Polská and the city center, mean risk was decreased by adjacent green areas (Figure 10, Table 11), thereby highlighting the advantage of assessing risk on a hexagon level. Nonetheless, most studies still use administrative boundaries for analysis (Buzási, 2022; Ellena et al., 2023; Räsänen et al., 2019; Savic et al., 2018; Voelkel et al., 2018), not least due to data only being available at a coarser spatial resolution. This issue also persists inside this study, where the spatial resolution of available datasets varied greatly. Especially the resolution of the census data with 1km was rather coarse to integrate it into a hexagonal grid, which is why dasymetric redistribution was applied here.

In the context of the spatial resolution of input datasets and limited computational power, the final length of each side of the hexagons was defined as 100m, which complies with many of the datasets used and similar studies conducted in Olomouc (Květoňová et al., 2025). Nonetheless, a higher spatial resolution of 20 to 40m is recommended for very detailed analysis (Pánek et al., 2019). Lehnert et al., 2021 have argued that a spatial resolution of 60m was too low to report thermal comfort and discomfort, which is why they decided on a final resolution of 30m. Similarly, the current map of the UHI adaptation strategy of Olomouc also has a spatial resolution of 30m, which made direct comparisons with the results achieved in this study difficult. It should therefore be considered to use an enhanced spatial resolution in the future.

Land Surface Temperature (LST)

To compute the hazard component of UHI risk, LST data acquired from satellites were seen as a crucial input. In this context, the initial goal was to use Landsat 8 and 9 data with a resampled spatial resolution of 30m as has been done in studies in Olomouc on thermal comfort (Lehnert et al., 2021, 2023). These scenes could then be combined with the ECOSTRESS module with a spatial resolution of 70m. This combination of the L2 product of ECOSTRESS and Landsat Collection 2 Level 2 on LST was used by Květoňová et al. (2024) for a study area in Prague.

While acquiring Landsat Collection 2 Level 2 data for Olomouc, it was found that all products had major data gaps in the study area, which is why this product could not be used in the analysis. As an alternative, Landsat Collection 2 Level 1 data could have been acquired and preprocessed manually. Contrary to Landsat Collection 2 Level 2 data, this data is not yet atmospherically corrected and LST first needs to be estimated with algorithms such as split window, which would have gone beyond the scope of this thesis.

Therefore, only ECOSTRESS LST scenes were integrated into the hazard component, where representative scenes without clouds were chosen for the summer period of 2025. Since the ECOSTRESS module acquires scenes both during the day and night, scenes were selected separately according to the daytime. To identify nocturnal UHII, following similar studies such as Lauwaet et al. (2024), pixels containing the lake area in the northern part of the city had to be masked out due to the lake's high specific heat capacity that strongly influenced the value range of nighttime UHII. Since the lake can have a positive effect on thermal comfort and the microclimate, especially for adjacent neighborhoods during the day, an alternative solution could be chosen in the future where the cooling effect of the lake is integrated into the final risk assessment.

Due to the varying temporal resolution of ECOSTRESS and the requirement of cloudless scenes, it should be noted that the dates of the daytime and nighttime scenes do not correspond to each other. Nonetheless, all scenes represent summer thermal conditions, where the daytime scenes were all acquired during heatwave events.

Sensor network data

The sensor network data from the ten weather stations was used to get temperature insights every few minutes. After all, the disadvantage of thermal data acquired from satellites is that the revisit time is rather low. On the other hand, the issue with the sensor data was the low number of stations that made interpolation impossible. At the same time, the sensors are distributed in areas with similar urban structure, which is why only a few LCZs were covered, resulting in a low thermal range. Additionally, the specific placement of the sensors is crucial as it can lead to mismatches between the urban structure and measured temperatures. In this context, the only weather station located within the compact midrise LCZ did not show the highest thermal metrics, even though this station represents the built-up core of the city and would therefore be expected to record the strongest heat signal. A possible explanation is the presence of blue infrastructure near this station, whose cooling effect may have offset the heat retention typically associated with this LCZ.

Since interpolation is currently not possible but might be in the future with an extension of the sensor network and distribution in all LCZs, satellite-derived hazard and air temperature indices were compared with each other to understand if the weather stations can provide additional insights that are currently not included in the risk model. While this comparison can provide a first indication, several problems arose in this context. First, hazard is calculated as a polygon layer while the temperature measurements are represented by points, leading to scale mismatches that made correlations and rankings between LST and air temperature difficult to grasp. As mentioned before, the low thermal range was another issue, as the small temperature differences between the stations made an accurate ranking from the highest and lowest value challenging. Nonetheless, this comparison still provided a useful starting point, offering an initial indication of where air temperature measurements might complement the current hazard layer once the sensor network is expanded.

Population Datasets

In the context of the exposure and sensitivity component, different population datasets were used to integrate various vulnerable population groups. While the address point layer has a very high spatial resolution and is one of the most recent datasets in this study, it only includes data on age groups, representing the vulnerable groups of children and the elderly. To gain additional insights into the distribution of women and people with a low educational status, census data were therefore used as an additional layer. Although this dataset is older and has a lower spatial resolution than address points, which is why it was also redistributed to the address points using a dasymetric method, this combination of datasets still enables the most informative output.

The issue with all these population datasets is that only permanent residents are considered, which is why whole population groups such as students or homeless people are not considered in the analysis. At the same time, these datasets are connected to the residency of the population and therefore do not consider the situation during the day when adults are at work and children go to kindergarten or school. To counteract this issue, the exposed population was here displayed with the population grid layer created by Rypl et al. (2026) that views population density separately during day and night. At the same time, schools and kindergartens were integrated as a separate vulnerable infrastructure layer to understand were children are staying during the day.

Indicator Overlaps and Redundancy

In general, certain indicators showed high correlations with each other, indicating overlaps and redundancy. This is especially the case for the indicators of vulnerable groups such as women and children whose spatial distribution is closely intertwined. Although these may indicate similar values in most hexagons resulting in high correlations, there is always a unique distribution in a certain number of hexagons that is crucial for UHI risk analysis. Still, to reduce this redundancy, the indicators of vulnerable groups were summarized into one final indicator instead of being considered separately.

Similarly, there are natural overlaps between the population distribution during day and night, which can result in an unconscious double weight in hexagons where population distribution is high during both day and night. Since this scenario increases especially the thermal stress on residents, this overlap is accepted in the scope of this study. The same applies to UHII during day and night, where both datasets show individual phenomena that contribute to UHI risk in different ways, which is why they are considered separately. This can again lead to a double weight when UHII is high both during the day and night, but this also naturally increases the real risk.

Lastly, both population distribution and UHII are available separately for daytime and nighttime, but are currently aggregated into a single risk score. This means hazard and exposure can combine into a high UHI risk score even when their peak values occur at different times of day, for example when daytime hazard is high, but the population is only concentrated in that area at night, or vice versa as commuters travel to and from the city for work. Since the current risk score does not distinguish when each component is actually at its highest, this temporal mismatch remains hidden. Analyzing UHI risk separately for daytime and nighttime could address this, though it would require additional data sources, as most currently available layers do not differentiate between day and night.

UHI Risk Model

For the conceptualization of the UHI risk model, the equation to calculate vulnerability had to be adapted from using the weighted arithmetic mean to using a multiplicative approach found in the literature (Voelkel et al., 2018). For the additive approach, especially the outskirts of the city distorted the overall risk score, where low adaptive capacity values combined with zero sensitivity resulted in moderate vulnerability values. With the multiplicative equation, vulnerability now only exists when sensitivity is more than zero, indicating that adaptive capacity can only reduce but not create vulnerability. For the final UHI risk assessment, this approach resulted in lower vulnerability values compared to hazard and exposure, which were calculated using the additive formula.

In general, the value ranges of final risk and its components varied, with hazard displaying higher values than exposure, which can be traced back to the varying number of indicators included in weighted arithmetic aggregation. A higher number of indicators here leads to more internal averaging that dampens extreme values. This is why each component was visualized individually using its own classification scheme based on natural breaks, rather than applying a uniform legend across all maps. Similarly, absolute values of risk and its components cannot be compared directly, but the relative spatial distribution of low and high values can still be analyzed.

Classification and Weighting of Indicators

Regarding the classification of indicators into the different risk components, this study aligns with recommendations from the literature, but the classification can vary depending on the study. Furthermore, this study is utilizing indicators on thermal comfort and discomfort that have not been used in UHI risk assessment before. The classification of these indicators is therefore based on subjective evaluation under consultation with experts from the university. While thermal comfort and discomfort are temperature datasets and they could therefore be considered as part of the hazard component, they were here assigned to vulnerability. This is due to their contradictory nature and their close connection to people's perception, where thermal discomfort shows how vulnerable residents are connected to heat and thermal comfort indicates areas that can increase the ability to cope with heat-related harm.

Lastly, UHI risk assessment is currently conducted using equal weights, but there is the option to adapt these weights in the created model. Many studies assign weights to specific indicators based on expert knowledge or methods such as Delphi or pairwise comparisons (Alonso & Renard, 2020; Räsänen et al., 2019). These weights could counteract the redundancy and overlapping of indicators and could also emphasize the most relevant indicators for UHI risk assessment. At the same time, it could be considered to assign higher weights to indicators that are only sparsely distributed but critical in certain locations, such as the vulnerable infrastructure indicator, which currently shows only low correlations with its component and final risk. Similarly, increased weighting could be placed on the vulnerability component itself, since its values are comparatively low as a result of the adapted multiplicative formula and a stronger emphasis on vulnerability could better reflect a people-centered approach.

8.2 Future Work

This UHI risk assessment is a first approach to identify priority zones for adaptation and mitigation strategies in Olomouc. The proposed methodology with the creation of a UHI risk model was consciously developed to be reproducible and transferable. In this context, the methodology can simply be repeated with the availability of additional data sources or a focus on a different study area.

Spatial Resolution and Study Area

Regarding the spatial framework, the spatial resolution of the hexagons could be improved to gain more detailed insights into the distribution of UHI risk in Olomouc. For computational stability with a refined spatial resolution of the hexagons, a smaller study area such as the city center could be focused instead of the whole city boundary. In this context, additional high-resolution data sets might be required. Depending on data availability, these could include heat-related deaths, paramedic incidents or also additional population datasets that do not only focus on permanent residents but instead consider mobile operator data.

Sensor Network Extension

A significant improvement could be the expansion of the sensor network in Olomouc, which is planned for the near future and will increase the number of sensors to up to 400, providing better coverage of different LCZs. This extension could enable the opportunity to integrate this layer into the actual UHI risk assessment by interpolating thermal metrics such as the number of hot days and warm nights or UHII acquired from air temperature measurements. These additional indicators could provide crucial insights into the hazard component that LST alone cannot provide.

Thermal Perception Data

As the integration of thermal perception data is part of the novelty of this study and shows satisfactory results with high correlations between thermal comfort and discomfort with its components, this data source could be further analyzed and enhanced. In this context, the participatory mapping results of the 2020 campaign could be filtered to responses of the older generation, thereby gaining specific insights into where the older generation feels thermally comfortable or uncomfortable. Similarly, additional methods such as thermal walks could be considered and integrated, which provide insights into the real-time evaluation of thermal conditions under controlled circumstances.

Weighting and UHI Risk Interpretation

Besides the improvement of data availability, the UHI risk assessment could be improved by adding a weighting scheme with individual weights for indicators and risk components based on consultation with experts. Similarly, enhancements could be made regarding the interpretation of UHI risk. In this context, statistical tests such as spatial autocorrelation could provide further insights into the distribution of UHI risk.

9 CONCLUSION

This study aimed to examine UHIs in Olomouc, a challenge that is becoming increasingly urgent for cities as heatwaves grow more frequent and severe. Since existing studies on UHIs tend to focus on objective measurements such as land surface or air temperature without considering how residents themselves experience and cope with heat, this thesis aimed to close this gap by developing a geospatial framework that combines objective thermal data with subjective thermal perception and socio-demographic vulnerability, thereby equally considering human perspective and physical heat patterns.

To achieve this, a hexagonal grid was established as a spatial framework independent of administrative boundaries, allowing thermal, urban and socio-demographic datasets of varying resolutions to be harmonized and compared consistently across the city. Building on the climate risk definition of the IPCC and the guidelines of the GIZ *Vulnerability Sourcebook*, UHI risk was conceptualized as a function of hazard, exposure and vulnerability, with the latter further divided into sensitivity and adaptive capacity. Hazard was derived from ECOSTRESS land surface temperature for day and night and exposure from urban structure and population density during day and night. While sensitivity was represented by vulnerable population groups, vulnerable infrastructure and reported thermal discomfort, adaptive capacity included urban green spaces, practitioners and reported thermal comfort. These indicators were normalized and combined using a reproducible script tool based on weighted arithmetic aggregation.

The results show that UHI risk is highest in and around the densely built-up city center, but that its underlying drivers vary considerably across Olomouc. Industrial and commercial zones are shaped primarily by high hazard from sealed surfaces, while residential neighborhoods such as Nové Sady and Povel stand out due to a high concentration of vulnerable population groups. These differentiated priority zones formed the basis for tailored recommendations, ranging from shading measures in the city center to early warning systems in vulnerable residential areas and heat-load mitigation in industrial zones. A comparison with the city's existing adaptation strategy further confirmed that this thesis captures socio-demographic vulnerability that purely physical susceptibility maps tend to overlook, underlining the added value of a human-centered perspective on UHI risk.

While most objectives of this thesis were achieved, its implementation also revealed aspects that could not yet be realized and instead point toward future research. Most notably, due to a small sample size of only ten weather stations distributed across similar LCZs, the sensor network data could not be integrated directly into the risk assessment and was instead used to validate the hazard component. Results here showed several discrepancies between LST and AT that indicate that the risk model could be further refined with the integration of the IoT network in the future with its extension. Beyond this, future work could focus on different spatial frameworks with finer hexagonal grids as well as on extending the current static assessment through the integration of climate models, allowing UHI risk and its corresponding recommendations to be projected for future scenarios rather than present conditions alone.

In summary, this thesis demonstrates that combining objective thermal data, urban structure, socio-demographic characteristics and subjective thermal perception provides a more holistic perspective on UHI risk. It was demonstrated that static maps on UHI risk and especially the interactive web mapping application can meaningfully support local decision-makers in prioritizing where mitigation and adaptation measures are most urgently needed. Given its reproducible design, the underlying model could further be transferred to other cities facing similar challenges. As climate change continues to intensify the frequency and severity of heatwaves and cities keep growing in population and density, integrating human perception and social vulnerability into UHI risk assessment will become even more important for building resilient and livable urban environments.

REFERENCES AND INFORMATION SOURCES

Abrar, R., Sarkar, S. K., Nishtha, K. T., Talukdar, S., Shahfahad, Rahman, A., Islam, A. R. M. T., & Mosavi, A. (2022). Assessing the Spatial Mapping of Heat Vulnerability under Urban Heat Island (UHI) Effect in the Dhaka Metropolitan Area. *Sustainability*, *14*(9), 4945. https://doi.org/10.3390/su14094945

Alonso, L., & Renard, F. (2019). Spatial comparison of the perception of urban heat islands and thermal comfort zones with participative in situ measurements and remote sensing data. https://generalisation.icaci.org/downloads/abs2019/Abs2019_paper_3.pdf

Alonso, L., & Renard, F. (2020). A Comparative Study of the Physiological and Socio-Economic Vulnerabilities to Heat Waves of the Population of the Metropolis of Lyon (France) in a Climate Change Context. *International Journal of Environmental Research and Public Health*, *17*(3), 1004. https://doi.org/10.3390/ijerph17031004

Bhattacharjee, S., Gerasimova, E., Imbert, C., Tencar, J., & Rotondo, F. (2019). Assessment of Different Methodologies for Mapping Urban Heat Vulnerability for Milan, Italy. *IOP Conference Series: Earth and Environmental Science*, *290*(1), 012162. https://doi.org/10.1088/1755-1315/290/1/012162

Buzási, A. (2022). Comparative assessment of heatwave vulnerability factors for the districts of Budapest, Hungary. *Urban Climate*, *42*, 101127. https://doi.org/10.1016/j.uclim.2022.101127

Canevari-Luzardo, L., Bastide, J., Choutet, I., & Liverman, D. (2017). Using partial participatory GIS in vulnerability and disaster risk reduction in Grenada. *Climate and Development*, *9*(2), 95–109. https://doi.org/10.1080/17565529.2015.1067593

Chen, Z.-Y., Achebak, H., Petetin, H., Méndez Turrubiates, R. F., Guo, Y., Pérez García-Pando, C., & Ballester, J. (2025). Trends in population exposure to compound extreme-risk temperature and air pollution across 35 European countries: A modelling study. *The Lancet Planetary Health*, *9*(5), e384–e396. https://doi.org/10.1016/S2542-5196(25)00048-8

Cheng, W., Li, D., Liu, Z., & Brown, R. D. (2021). Approaches for identifying heat-vulnerable populations and locations: A systematic review. *Science of The Total Environment*, *799*, 149417. https://doi.org/10.1016/j.scitotenv.2021.149417

Cheval, S., Amihăesei, V.-A., Chitu, Z., Dumitrescu, A., Falcescu, V., Irașoc, A., Micu, D. M., Mihulet, E., Ontel, I., Paraschiv, M.-G., & Tudose, N. C. (2024). A systematic review of urban heat island and heat waves research (1991–2022). *Climate Risk Management*, *44*, 100603. https://doi.org/10.1016/j.crm.2024.100603

CiTiQ & EnCLOD (2026). IoT Register. Meteorologická data Olomouc. https://iot.citiq.cloud/portal/docs/meteorological-data-olomouc/

Climate-Data.org (2026). Olomouc Climate (Czech Republic). Data and graphs for weather & climate in Olomouc. https://en.climate-data.org/europe/czech-republic/olomouc/olomouc-6272/

Copernicus Land Monitoring Service (CLMS) (2021a). Urban Atlas Land Cover/Land Use 2021 (vector), Europe, 3-yearly. https://doi.org/10.2909/05ae1ee1-e550-4e66-b74d-4926322d981a

Copernicus Land Monitoring Service (CLMS). (2021b). Urban Atlas Street Tree Layer 2021 (vector), Europe, 3-yearly. https://doi.org/10.2909/ed0018c3-5ad0-4721-b5e4-0042aeaf9d00

Crichton, D. (1999). The risk triangle. *Natural disaster management*, *102*(3), 102-103.

Czech Data Portal (2026a). National Register of Healthcare Providers (Dataset). https://data.gov.cz/dataset?iri=https%3A%2F%2Fdata.gov.cz%2Fzdroj%2Fdatov%C3%A9-sady%2F00025593%2F33a742e51c1ac89c1a17008084e2412e

Czech Data Portal (2026b). Population grid of the Czech Republic (Dataset). https://data.gov.cz/datov%C3%A1-sada?iri=https%3A%2F%2Fdata.gov.cz%2Fzdroj%2Fdatov%C3%A9-sady%2F00020699%2F5adb92c1679e653c68156c04ce10c0d5

Czech Hydrometeorological Institute (CHMI) (2026). Meteorological data measured in the network of CHMI stations for the current year at an interval of 10 minutes (Dataset). https://data.gov.cz/datov%C3%A1-sada?iri=https%3A%2F%2Fdata.gov.cz%2Fzdroj%2Fdatov%C3%A9-sady%2F00020699%2F5adb92c1679e653c68156c04ce10c0d5

Czech Statistical Office (CZSO) (2021). Olomouc (district Olomouc). Census 2021. https://vdb.czso.cz/vdbvo2/faces/en/index.jsf?page=profil-uzemi&uzemiprofil=34055&u=__VUZEMI__43__500496

Czech Statistical Office (CZSO) (2024). Olomouc (district Olomouc). Selected data about municipality. https://vdb.czso.cz/vdbvo2/faces/en/index.jsf?page=profil-uzemi&uzemiprofil=31588&u=__VUZEMI__43__500496#profil31591=page%3Dpozice-profilu%26rqup%3DA%26pvo%3DPU-MOSZV-01%26z%3DT%26f%3DTABULKA%26clsp%3D31591%26katalog%3D31591

Czech Statistical Office (CZSO) (2025). Number of inhabitants in municipalities - as of 1. 1. 2025. https://csu.gov.cz/produkty/pocet-obyvatel-v-obcich-rlm0s92pwn

de Groot-Reichwein, M. A. M., van Lammeren, R. J. A., Goosen, H., Koekoek, A., Bregt, A. K., & Vellinga, P. (2018). Urban heat indicator map for climate adaptation planning. *Mitigation and Adaptation Strategies for Global Change*, *23*(2), 169–185. https://doi.org/10.1007/s11027-015-9669-5

Dobrovolný, P., & Krahula, L. (2015). The spatial variability of air temperature and nocturnal urban heat island intensity in the city of Brno, Czech Republic. *Moravian Geographical Reports*, *23*(3), 8–16. https://doi.org/10.1515/mgr-2015-0013

Earth Resources Observation and Science (EROS) Center. (2020). *Landsat 8-9 Operational Land Imager / Thermal Infrared Sensor Level-2, Collection 2 [dataset]. U.S. Geological Survey*. https://doi.org/10.5066/P9OGBGM6.

Ellena, M., Melis, G., Zengarini, N., Di Gangi, E., Ricciardi, G., Mercogliano, P., & Costa, G. (2023). Micro-scale UHI risk assessment on the heat-health nexus within cities by looking at socio-economic factors and built environment characteristics: The Turin case study (Italy). *Urban Climate*, *49*, 101514. https://doi.org/10.1016/j.uclim.2023.101514

Fabrizi, R., Bonafoni, S., & Biondi, R. (2010). Satellite and Ground-Based Sensors for the Urban Heat Island Analysis in the City of Rome. *Remote Sensing*, *2*(5), 1400–1415. https://doi.org/10.3390/rs2051400

Fekih, M., Bechkit, W., Rivano, H., Dahan, M., Renard, F., Lucille, A., & Pineau, F. (2020). Participatory Air Quality and Urban Heat Islands Monitoring System. *IEEE Transactions on Instrumentation and Measurement*, *PP*, 1–1. https://doi.org/10.1109/TIM.2020.3034987

Geiger, R. (1961). Überarbeitete Neuausgabe von Geiger, R. Köppen Geiger/Klima der Erde. (Wandkarte 1:16 Mill.)

Geletič, J., & Vysoudil, M. (2012). Analysis of surface temperatures in urban and suburban landscapes from satellite thermal images: A case study of Olomouc and its environs, Czech Republic. *Moravian Geographical Reports*, *20*, 2–15. https://geography.upol.cz/soubory/lide/vysoudil/citace/jimp/2012_MGR.pdf

GIZ, & EURAC. (2017). Risk Supplement to the Vulnerability Sourcebook. Guidance on how to apply the Vulnerability Sourcebook's approach with the new IPCC AR5 concept of climate risk. Bonn: GIZ. https://www.adaptationcommunity.net/wp-content/uploads/2017/10/GIZ-2017_Risk-Supplement-to-the-Vulnerability-Sourcebook.pdf

GIZ. (2014). The Vulnerability Sourcebook Concept and guidelines for standardised vulnerability assessments. https://health.bmz.de/wp-content/uploads/page/Vulnerability_Sourcebook__1_.pdf

Google. (2026). Google Maps Street View imagery. Retrieved July 24, 2026, from https://www.google.com/maps

Guerreiro, S. B., Dawson, R. J., Kilsby, C., Lewis, E., & Ford, A. (2018). Future heat-waves, droughts and floods in 571 European cities. *Environmental Research Letters*, *13*(3), 034009. https://doi.org/10.1088/1748-9326/aaaad3

Hook, S., & Hulley, G. (2023). ECOSTRESS Gridded Land Surface Temperature and Emissivity Instantaneous L2 Global 70 m v002 [Dataset]. NASA Land Processes Distributed Active Archive Center. https://doi.org/10.5067/ECOSTRESS/ECO_L2G_LSTE.002 Date Accessed: 2026-07-29

IPCC (2007). *Climate Change 2007: Synthesis Report. Contribution of Working Groups I, II and III to the Fourth Assessment Report of the Intergovernmental Panel on Climate Change* [Core Writing Team, Pachauri, R.K and Reisinger, A. (eds.)]. IPCC, Geneva, Switzerland, 104 pp.

IPCC (2014) *Climate Change 2014: Synthesis Report. Contribution of Working Groups I, II and III to the Fifth Assessment Report of the Intergovernmental Panel on Climate Change* [Core Writing Team, R.K. Pachauri and L.A. Meyer (eds.)]. IPCC, Geneva, Switzerland, 151 pp.

Jang, S., Bae, J., & Kim, Y. (2024). Street-level urban heat island mitigation: Assessing the cooling effect of green infrastructure using urban IoT sensor big data. *Sustainable Cities and Society*, *100*, 105007. https://doi.org/10.1016/j.scs.2023.105007

Kamath, H. G., Martilli, A., Singh, M., Brooks, T., Lanza, K., Bixler, R. P., Coudert, M., Yang, Z.-L., & Niyogi, D. (2023). Human heat health index (H3I) for holistic assessment of heat hazard and mitigation strategies beyond urban heat islands. *Urban Climate*, *52*, 101675. https://doi.org/10.1016/j.uclim.2023.101675

Kirschner, V., Urban, A., Chlapcová, L., & Řezáčová, V. (2025). Thermal comfort perception among park users in Prague, Central Europe on hot summer days—A comparison of thermal indices. *PLOS ONE*, *20*(1), e0299377. https://doi.org/10.1371/journal.pone.0299377

Krkoška Lorencová, E., Whitham, C. E. L., Bašta, P., Harmáčková, Z. V., Štěpánek, P., Zahradníček, P., Farda, A., & Vačkář, D. (2018). Participatory Climate Change Impact Assessment in Three Czech Cities: The Case of Heatwaves. *Sustainability*, *10*(6), 1906. https://doi.org/10.3390/su10061906

Květoňová, V., Pánek, J., Geletič, J., Šimáček, P., & Lehnert, M. (2024). Where is the heat threat in a city? Different perspectives on people-oriented and remote sensing methods: The case of Prague. *Heliyon*, *10*(16), e36101. https://doi.org/10.1016/j.heliyon.2024.e36101

Květoňová, V., Pánek, J., Koníček, J., & Lehnert, M. (2025). Wintertime thermal perception in a central European city: The case of Olomouc, Czechia. *Journal of Maps*, *21*(1), 2537687. https://doi.org/10.1080/17445647.2025.2537687

Lang, S., Kienberger, S., Tiede, D., Hagenlocher, M., & Pernkopf, L. (2014). Geons – domain-specific regionalization of space. *Cartography and Geographic Information Science*, *41*(3), 214–226. https://doi.org/10.1080/15230406.2014.902755

Lauwaet, D., Berckmans, J., Hooyberghs, H., Wouters, H., Driesen, G., Lefebre, F., & De Ridder, K. (2024). High resolution modelling of the urban heat island of 100 European cities. *Urban Climate*, *54*, 101850. https://doi.org/10.1016/j.uclim.2024.101850

Lehnert, M., Geletič, J., Kopp, J., Brabec, M., Jurek, M., & Pánek, J. (2021). Comparison between mental mapping and land surface temperature in two Czech cities: A new perspective on indication of locations prone to heat stress.

Building and Environment, *203*, 108090. https://doi.org/10.1016/j.buildenv.2021.108090

Lehnert, M., Janků, Z., Novotný, D., Jurek, M., & Geletič, J. (2025). Assessment of air temperature indices and urban heat island intensity based on two meteorological networks in Prague, Czechia. *Theoretical and Applied Climatology*, *156*(9), 470. https://doi.org/10.1007/s00704-025-05707-5

Lehnert, M., Kubeček, J., Geletič, J., Jurek, M., & Frajer, J. (2018). Identifying hot and cool spots in the city centre based on bicycle measurements: The case of Olomouc, Czech Republic. *Geographica Pannonica*, *22*(4), 230–240. https://doi.org/10.5937/gp22-19750

Lehnert, M., Pánek, J., Kopp, J., Geletič, J., Květoňová, V., & Jurek, M. (2023). Thermal comfort in urban areas on hot summer days and its improvement through participatory mapping: A case study of two Central European cities. *Landscape and Urban Planning*, *233*, 104713. https://doi.org/10.1016/j.landurbplan.2023.104713

Lim, T. C., Wilson, B., Grohs, J. R., & Pingel, T. J. (2022). Community-engaged heat resilience planning: Lessons from a youth smart city STEM program. *Landscape and Urban Planning*, *226*, 104497. https://doi.org/10.1016/j.landurbplan.2022.104497

Meng, X., Fei, M., Zhao, Z., & Yin, C. (2021). Prediction of Urban Heat Island Effect over Jinan City Using the Markov-Cellular Automata Model Combined with Urban Biophysical Descriptors. *Journal of the Indian Society of Remote Sensing*, *49*, 997–1009. https://doi.org/10.1007/s12524-020-01274-6

Ming, Y., Liu, Y., Liu, X., & Tian, Z. (2024). Demographic disparity in diurnal surface urban Heat Island exposure across local climate zones: A case study of Chongqing, China. *Science of The Total Environment*, *923*, 171203. https://doi.org/10.1016/j.scitotenv.2024.171203

Oke, T. (1982). The energetic basis of urban heat island. *Quarterly Journal of the Royal Meteorological Society*, *108*, 1–24. https://doi.org/10.1002/qj.49710845502

Oke, T. R. (1973). City size and the urban heat island. *Atmospheric Environment (1967)*, *7*(8), 769–779. https://doi.org/10.1016/0004-6981(73)90140-6

Oke, T. R. (1976). The distinction between canopy and boundary-layer urban heat islands. *Atmosphere*, *14*(4), 268–277. https://doi.org/10.1080/00046973.1976.9648422

Oke, T. R., Mills, G., Christen, A., & Voogt, J. A. (2017). *Urban climates*. Cambridge University Press. https://doi.org/10.1017/9781139016476

OpenStreetMap contributors. (2026). OpenStreetMap. https://www.openstreetmap.org

Pánek, J. (2019). Mapping citizens' emotions: Participatory planning support system in Olomouc, Czech Republic. *Journal of Maps*, *15*(1), 8–12. https://doi.org/10.1080/17445647.2018.1546624

Pánek, J., Ivan, I., & Macková, L. (2019). Comparing Residents' Fear of Crime with Recorded Crime Data—Case Study of Ostrava, Czech Republic. *ISPRS International Journal of Geo-Information*, *8*(9), 401. https://doi.org/10.3390/ijgi8090401

Quesada-Ganuza, L., Garmendia, L., Alvarez, I., & Roji, E. (2023). Vulnerability assessment and categorization against heat waves for the Bilbao historic area. *Sustainable Cities and Society*, *98*, 104805. https://doi.org/10.1016/j.scs.2023.104805

Räsänen, A., Heikkinen, K., Piila, N., & Juhola, S. (2019). Zoning and weighting in urban heat island vulnerability and risk mapping in Helsinki, Finland. *Regional Environmental Change*, *19*(5), 1481–1493. https://doi.org/10.1007/s10113-019-01491-x

Reinwald, F., Thiel, S., Kainz, A., & Hahn, C. (2024). Components of urban climate analyses for the development of planning recommendation maps. *Urban Climate*, *57*, 102090. https://doi.org/10.1016/j.uclim.2024.102090

Rodrigues de Almeida, C., Teodoro, A. C., & Gonçalves, A. (2021). *Study of the Urban Heat Island (UHI) Using Remote Sensing Data/Techniques: A Systematic Review*. https://www.mdpi.com/2076-3298/8/10/105

Rypl, O., Dobešová, Z., & Burian, J. (2026). Representative population distribution layer for Czechia: From methodology to automated solutions. *International Journal of Digital Earth*, *19*(1), 2616577. https://doi.org/10.1080/17538947.2026.2616577

Savic, S., Marković, V., Secerov, I., Pavic, D., Arsenovic, D., Milosevic, D., Dolinaj, D., Nagy, I., & Pantelić, M. (2018). Heat wave risk assessment and mapping in urban areas: Case study for a mid-sized Central European city, Novi Sad (Serbia). *Natural Hazards*, *91*, 891–911. https://doi.org/10.1007/s11069-017-3160-4

Sidiqui, P., Roös, P. B., Herron, M., Jones, D. S., Duncan, E., Jalali, A., Allam, Z., Roberts, B. J., Schmidt, A., Tariq, M. A. U. R., Shah, A. A., Khan, N. A., & Irshad, M. (2022). Urban Heat Island vulnerability mapping using advanced GIS data and tools. *Journal of Earth System Science*, *131*(4), 266. https://doi.org/10.1007/s12040-022-02005-w

Steadman, R.G., 1994. Norms of apparent temperature in Australia. *Aust. Meteorol. Mag.*, 43, pp.1–16.

Stewart, I. D., & Oke, T. R. (2012). Local Climate Zones for Urban Temperature Studies. *Bulletin of the American Meteorological Society*, *93*(12), 1879–1900. https://doi.org/10.1175/BAMS-D-11-00019.1

Středová, H., Chuchma, F., Rožnovský, J., & Středa, T. (2021). Local Climate Zones, Land Surface Temperature and Air Temperature Interactions: Case Study of Hradec Králové, the Czech Republic. *ISPRS International Journal of Geo-Information*, *10*(10), 704. https://doi.org/10.3390/ijgi10100704

Sullivan-Wiley, K. A., Short Gianotti, A. G., & Casellas Connors, J. P. (2019). Mapping vulnerability: Opportunities and limitations of participatory community mapping. *Applied Geography*, *105*, 47–57. https://doi.org/10.1016/j.apgeog.2019.02.008

Szagri, D., Nagy, B., & Szalay, Z. (2023). How can we predict where heatwaves will have an impact? – A literature review on heat vulnerability indexes. *Urban Climate*, *52*, 101711. https://doi.org/10.1016/j.uclim.2023.101711

Thanvisitthpon, N. (2023). Statistically Validated Urban Heat Island Risk Indicators for UHI Susceptibility Assessment. *International Journal of Environmental Research and Public Health*, *20*, 1172. https://doi.org/10.3390/ijerph20021172

Tzavali, A., Paravantis, J. P., Mihalakakou, G., Fotiadi, A., & Stigka, E. (2015). *Urban heat island intensity: A literature review*. ResearchGate. https://www.researchgate.net/publication/298083233_Urban_heat_island_intensity_A_literature_review

UNDRR. (2026). *Record-breaking heat spreads through Europe | PreventionWeb*. Retrieved 29 June 2026, https://www.preventionweb.net/news/record-breaking-heat-spreads-through-europe

United Nations. (2026). *Goal 11 | Department of Economic and Social Affairs*. Retrieved 30 June 2026, from https://sdgs.un.org/goals/goal11#targets_and_indicators

Vaňo, S., Duchková, H., Bašta, P., Jančovič, M., Geletič, J., Lorencová, E. K., & Suchá, L. (2025). From scenarios to strategies: Integrated methodology for addressing urban heat vulnerability in an uncertain future. *Sustainable Cities and Society*, *121*, 106202. https://doi.org/10.1016/j.scs.2025.106202

Varquez, A. C. G., Taerakul, J., Renard, F., Alonso, L., Choi, S., Hiroki, R., Ashie, Y., Kumakura, E., Okumura, M., Hanaoka, S., Inagaki, A., & Kanda, M. (2025). High-resolution outdoor heat-risk modeling for city central areas with applications to Tokyo and Lyon. *Sustainable Cities and Society*, *125*, 106344. https://doi.org/10.1016/j.scs.2025.106344

Vizina, I. Š., Jedlička, I. J., Kantor, I. Č., Jurečka, I. F., & Ausficír, B. J. (2020). ADAPTACNÍ A MITIGACNÍ STRATEGIE MESTA OLOMOUCE. Analytická čast – Záveřečná zpráva.

https://www.olomouc.eu/administrace/repository/gallery/articles/24_/24763/adaptacni-a-mitigacni-strategie.cs.pdf?srsltid=AfmBOoqN_TjcuXS-ZL0PdhuH1B-7j74VLz7mV-gXa8y15Mmcv6HNkaz_

Voelkel, J., Hellman, D., Sakuma, R., & Shandas, V. (2018). Assessing Vulnerability to Urban Heat: A Study of Disproportionate Heat Exposure and Access to Refuge by Socio-Demographic Status in Portland, Oregon. *International Journal of Environmental Research and Public Health*, *15*(4), 640. https://doi.org/10.3390/ijerph15040640

Voogt, J. A., & Oke, T. R. (2003). Thermal remote sensing of urban climates. *Remote Sensing of Environment, Urban Remote Sensing*, *86*(3), 370–384. https://doi.org/10.1016/S0034-4257(03)00079-8

Wagner, M., Květoňová, V., Jirmus, R., & Lehnert, M. (2025). Towards greener cities: Evaluating urban green space accessibility using the 3-30-300 rule exampled on the city of Olomouc (Czech Republic). *Moravian Geographical Reports*, *33*(2), 129–142. https://doi.org/10.2478/mgr-2025-0010

Wei, L., & Sobrino, J. A. (2024). Surface urban heat island analysis based on local climate zones using ECOSTRESS and Landsat data: A case study of Valencia city (Spain). *International Journal of Applied Earth Observation and Geoinformation*, *130*, 103875. https://doi.org/10.1016/j.jag.2024.103875

Wu, H., Xu, Y., Zhang, M., Su, L., Wang, Y., & Zhu, S. (2024). Spatially explicit assessment of the heat-related health risk in the Yangtze River Delta, China, using multisource remote sensing and socioeconomic data. *Sustainable Cities and Society*, *104*, 105300. https://doi.org/10.1016/j.scs.2024.105300

Xu, C., Wei, R., & Tong, H. (2025). A Systematic Review of Methodological Advances in Urban Heatwave Risk Assessment: Integrating Multi-Source Data and Hybrid Weighting Methods. *Sustainability*, *17*(8), 3747. https://doi.org/10.3390/su17083747

Žgela, M., Vavassori, A., & Brovelli, M. A. (2025). Predicting Air Temperature Patterns in Milan Using Crowdsourced Measurements and Earth Observation Data. *Remote Sensing*, *17*(21), 3520. https://doi.org/10.3390/rs17213520

Note on the Use of AI and Language Tools

For this thesis, ChatGPT and Claude were used to organize ideas into a coherent structure and to improve the sentence structure. Claude was used to assist with script writing and debugging, including the R scripts, the Python/ArcPy script underlying the UHI risk assessment toolbox and the Google Colab notebook. DeepL and Grammarly were applied to enhance the language quality by correcting spelling and grammatical errors.

ATTACHMENTS

LIST OF ATTACHMENTS

Free attachments

Attachment 1 Poster
Attachment 2 Web Mapping Application
Attachment 3 Website
Attachment 4 Digital Data

The poster and map gallery with all presented maps in high resolution can be found on the website:
https://www.geoinformatics.upol.cz/dprace/magisterske/kiefer26/

The web mapping application can be found here:
https://experience.arcgis.com/experience/bd0cb55005cf4592a6a077444d34ed48

The reproducible ArcGIS Pro toolbox with the UHI risk model can be found here:
https://github.com/annabellekiefer/UHI_Risk_Assessment